

MINES
LIBRARY
Thesis
3508

University of Nevada

The City of Reno, Nevada
Reno

Fundamental Studies on Electrochemical Processing
of Light Weight Alloys

A thesis submitted in partial fulfillment of the requirements for the degree of

Master of Science in Metallurgical Engineering

by

Palani T. Velu

Professor Ramana G. Reddy
Thesis Advisor

May 1995

UNIVERSITY LIBRARY
UNIVERSITY OF NEVADA, RENO
RENO, NV 89557

2557514

IUMI 11/95 7

The thesis of Palani T. Velu is approved:

I express my deep sense of gratitude and thanks to Dr. Ramana G. Reddy for his
continued supervision, encouragement and advice during my studies and the course covered
of this project. I gratefully acknowledge Dr. G. Rantala and Dr. Y.A. Cengel for their
advice, Dr. G. Rantala and Dr. Y.A. Cengel for their

Ramana Reddy

Thesis Advisor

the course. I am highly indebted to my friend, Dr. Suresh G. Kulkarni for his moral
support and encouragement throughout the course.

Ross W. Smith

Department Chair

and Mr. M.L. Mendenhall, Mr. A.M. Salinas, Mr. G. Thomas and Mr. G. Mullin,
during the past few years.

Rud C. Deery

Dean, Graduate School

University of Nevada

Reno

May 1995

ACKNOWLEDGEMENTS

I express my deep sense of gratitude and thanks to Dr. Ramana G. Reddy for his constant supervision, encouragement and advice during my studies and the entire course of this project. I gratefully acknowledge Dr. R.G. Bautista and Dr. Y.A. Cengel for their advice, criticism and interest in this work.

I express my sincere thanks to all my brothers for their encouragement throughout my career. I am highly indebted to my friend, Dr. Sampath G. Kumar for his moral support, encouragement, help, lively discussions and advice in carrying out my studies and research. I appreciate the help and support of my friends, Dr. S. Wang, Mr. K.S. Rao, Mr. H.H. Mandalia, Mr. A.M. Raichur, Mr. D. Mahesh and Mr. G. Madhu, during the past two years.

Finally, my sincere thanks and appreciation to the Dept. of Chemical and Metallurgical Engineering and National Science Foundation for providing financial assistance during my studies at UNR.

ABSTRACT

The electrochemical synthesis of aluminum-lithium alloys by a novel in-situ processing was investigated. The electrolyte used was LiF-CaF_2 with lithium compounds, Li_2O and Li_2CO_3 . Lithium obtained by dissociation of its compounds deposited into the liquid aluminum cathode at the bottom. The fundamental parameters studied were: (1) solubility of lithium compounds; (2) anodic overvoltages of LiF-CaF_2 electrolyte; (3) Liquidus temperatures of the electrolytes. The solubility was found to increase from 11.42 wt % at 1078 K to 14.77 wt % at 1133 K for Li_2O . For Li_2CO_3 it increased from 2.95 wt % at 1063 K to 7.57 wt % at 1093 K. Anodic overvoltages were measured as a function of current density and reaction mechanisms were analyzed. A limiting current density phenomenon was observed at 0.011 A/cm^2 for the $\text{LiF-CaF}_2\text{-Li}_2\text{CO}_3$ and at 0.52 A/cm^2 for $\text{LiF-CaF}_2\text{-Li}_2\text{O}$ systems. The liquidus temperatures of the electrolyte saturated with the lithium compounds were determined.

CONTENTS

Section	Description	Page
	ACKNOWLEDGEMENTS	ii
	ABSTRACT	iii
	CONTENTS	iv
	LIST OF TABLES	vi
	LIST OF FIGURES	vii
1.	INTRODUCTION	1
2.	LITERATURE REVIEW	3
	2.1. Alloy Development	7
	2.2. Processing Methods	11
	2.3. Solubility of Oxides and Chlorides in Halide Melts	13
	2.4. Electrochemical Production of Metals and Alloys from Halide Melts	16
3.	SOLUBILITY OF LITHIUM OXIDE AND LITHIUM CARBONATE IN LiF-CaF ₂ MELTS	22
	3.1. Theoretical Background	22
	3.2. Experimental Studies	22
	3.2.1. Materials used	25
	3.2.2. Experimental Procedure	25
	3.2.3. EMF measurements	29
	3.2.4. Procedure for Liquidus Temperatures	30

	v
3.3. Results and Discussion	32
3.3.1. Solubility of Lithium Oxide	32
3.3.2. Activity of Li_2O in the Melt	38
3.3.3. Solubility of Lithium Carbonate	43
3.3.4. Activity of Li_2CO_3 in the Melt	43
3.3.5. Liquidus Temperatures	50
4. ANODIC OVERVOLTAGE MEASUREMENTS DURING THE ELECTROLYSIS OF LITHIUM COMPOUNDS IN THE LiF-CaF_2 MELTS	55
4.1. Theoretical Background	55
4.2. Experimental Studies	56
4.3. Results and Discussion	60
4.3.1. Overvoltage of $\text{LiF-CaF}_2 + \text{Li}_2\text{CO}_3$ System	60
4.3.2. Determination of Oxyfluoride Complex	70
4.3.3. Overvoltage of $\text{LiF-CaF}_2 + \text{Li}_2\text{O}$ System	73
5. COMPARISON OF $\text{LiF-CaF}_2 + \text{Li}_2\text{CO}_3$ AND $\text{LiF-CaF}_2 + \text{Li}_2\text{CO}_3$ SYSTEMS	79
5.1. Solubility and Liquidus Temperatures	79
5.2. Liquidus Temperatures	79
5.3. Anodic Overvoltages	80
6. SUMMARY AND CONCLUSIONS	81
7. SCOPE FOR FUTURE WORK	83
REFERENCES	85
APPENDIX - A	90
APPENDIX - B	93

LIST OF TABLES

No.	TITLE	PAGE
1.	Mechanical Properties of Different Aluminum Alloys	5
2.	Densities of Different Aluminum Alloys	6
3.	Design Properties of Alloys Considered for Replacement by Al-Li Alloys	8
4.	Nominal Compositions of Different Aluminum-Lithium Alloys	10
5.	Solubilities of Various Oxides in Fluoride Electrolytes	17
6.	Solubilities of Various Chlorides in Chloride Electrolytes	18
7.	Solubilities of Li_2O by both EMF and Chemical Analysis Method	36
8.	Activity and Activity Coefficient of Li_2O in the Electrolyte at Various Temperatures	40
9.	Temkin Activity Coefficients of Li_2O in the Melt	42
10.	Solubilities of Li_2CO_3 at Various Temperatures	47
11.	Temkin Activities of Li_2CO_3 in the Electrolyte	51
12.	Liquidus Temperatures of Different Electrolyte Systems	53
13.	Anodic Overvoltage Measurements for Li_2O System at 1093 K	61
14.	Calculated Values of $1/i$ and $\text{Exp}(-F\eta / RT)$ for the Li_2O System	68
15.	Anodic Overvoltage Measurements for Li_2CO_3 System at 1093 K	74
16.	Calculated Values of $1/i$ and $\text{Exp}(-F\eta / RT)$ for the Li_2CO_3 System	76

LIST OF FIGURES

No.	TITLE	PAGE
1.	Aluminum-lithium Phase Diagram	23
2.	LiF-CaF ₂ Phase Diagram	24
3.	Sectional view of the Experimental Setup	26
4.	Schematic Diagram of the Argon Gas Cleaning Setup	28
5.	Schematic Diagram of the EMF Measurement Setup	31
6.	EMF Vs Wt. percent of Li ₂ O Dissolved at 1078 K	33
7.	EMF Vs Wt. percent of Li ₂ O Dissolved at 1113 K	34
8.	EMF Vs Wt. percent of Li ₂ O Dissolved at 1133 K	35
9.	Variation of $\ln X_{Li_2O}$ with Temperature	37
10.	EMF Vs Wt. percent of Li ₂ CO ₃ Dissolved at 1063 K	44
11.	EMF Vs Wt. percent of Li ₂ CO ₃ Dissolved at 1083 K	45
12.	EMF Vs Wt. percent of Li ₂ CO ₃ Dissolved at 1093 K	46
13.	Variation of $\ln X_{Li_2CO_3}$ with Temperature	48
14.	Solubilities of Different Oxides in Fluoride Melts	52
15.	Liquidus Temperature of LiF-CaF ₂ - Li ₂ CO ₃ (sat.) Melt	54
16.	Schematic Diagram of the Overvoltage Measurement Setup	57
17.	Schematic Outline of the Electric Circuit for Overvoltage Measurements	58

I. INTRODUCTION

18. Variation of Overvoltage Vs Log Current Density on Graphite Anode During Electrolysis of $\text{LiF-CaF}_2 + \text{Li}_2\text{CO}_3(\text{sat.})$ Melt at 1093 K 62
19. Variation of the Factor $\text{Exp}(-F\eta / RT)$ with Current Density at 1093 K for Li_2CO_3 Saturated System 69
20. Variation of Overvoltage Vs Log Current Density on Graphite Anode During Electrolysis of $\text{LiF-CaF}_2 + \text{Li}_2\text{O}(\text{sat.})$ Melt at 1093 K 75
21. Variation of the Factor $\text{Exp}(-F\eta / RT)$ with Current Density at 1093 K for Li_2O Saturated System 77

1. INTRODUCTION

Light weight aluminum alloys are one of the important structural materials that will play a crucial role in the construction of 21st century automobiles and aerospace systems. Al-Li alloys are being predicted to take the lion's share in this vast market. Currently, the switch over to Al-Li alloys for the components and structures are taking place at a slow pace. However, regardless of the timing, there appears to be a determined shift to the Al-Li alloys because of the potential weight savings. If these alloys were used throughout a Boeing 747, the total weight would be reduced by 10,000 lbs (4545 kgs)[1]. Recently, the automobile giant, Chrysler Corporation has built an experimental aluminum automobile that weighs 2000 lbs (900 kgs) compared to 2625 lbs (1200 kgs) for the conventional automobile of the same class[2].

The decrease in the dead weight of aircrafts and automobiles, as in these examples, decreases the fuel consumption and thereby increases the efficiency. In addition to weight savings, there are other advantages in using Al-Li alloys for their mechanical properties. The density of Al-Li alloys is 8 to 10 % lower and the modulus of elasticity is 10 to 12 % higher than that of conventional 2XXX and 7XXX alloys[3]. Due to these advantages, the commercial exploitation of Al-Li alloys have been investigated by many researchers[4-9]. The demand for the Al-Li alloys requirement is increasing mainly due to the following factors: (1) continuous increase in the fuel costs; (2) increased urge to reduce fuel consumption and increase the fuel efficiency; (3) improved mechanical properties of Al-Li alloys; (4) its extensive previous use in structures without any major problems and the availability manufacturing facilities.

There are two major process routes adopted currently for the commercial production of Al-Li alloys. They are:- (1) melting aluminum combined with pure lithium and casting into ingots or direct chilled semi-continuous rods[5,6]; (2) powder metallurgy techniques utilizing elemental or alloy powders[7-9]. Both of these methods have various disadvantages such as high energy consumption, utilization of expensive pure lithium and inferior mechanical properties of the final alloy. A new process has been investigated to overcome these demerits and prepare lithium by in-situ electrolysis of lithium compounds into Al-Li alloys in molten electrolytes. Lithium is mainly produced from ores either in the form of pure element or as lithium carbonate. The current market price of pure lithium in the less expensive product form is \$ 37.00 per 100 g. The price of Li_2CO_3 is \$ 3.90 and LiOH is \$ 21.90 per 100 g each[10]. The high price of pure lithium is due to the concentration of lithium from the minerals and the processing costs involved in separating it. Therefore, the process investigated here, utilizing low cost lithium compounds, is highly economical in producing Al-Li alloys.

The principal objective of the research work presented here is to generate physico-chemical data and to apply this information in the direct production of Al-Li alloys by electrolysis. The following fundamental information were determined by experimental investigation: (1) liquidus temperature of LiF-CaF_2 electrolyte saturated with Li_2CO_3 ; (2) the solubility of Li_2O and Li_2CO_3 separately in the LiF-CaF_2 electrolyte as a function of temperature; (3) the anodic overvoltage on graphite electrode during electrolysis with current density levels; (4) thermodynamic properties like activities from solubility data; (5) a comparison between Li_2O and Li_2CO_3 systems was made.

2. LITERATURE REVIEW

It is now well established that Petroleum reserves are not inexhaustible. Therefore, efforts to conserve the energy resources, resulted in the continuous increase in the fuel costs. The steep escalation of fuel costs since 1970's necessitated the manufacturers of automobiles and aircrafts always in the run looking for low density high strength materials. This class of materials offer the unique advantage of overall weight reduction in the structure. The weight reduction is the major technological option for improving the fuel economy of the vehicles. As the requirement for improvements in weight reduction increases day by day, other properties of the materials such as specific strength and specific stiffness becomes critical for the performance of the vehicles. In this respect, the aluminum and its alloys offer unique advantages.

Aluminum and its alloys are a class of versatile light materials. The properties they possess make them being used widely in the transportation, food and beverage, packaging, electrical and construction industries. The transportation and construction industries are the major users of large quantities of wrought heat treatable aluminum alloys. The other industries use mainly pure aluminum and non-heat treatable castings and alloys. These heat treatable aluminum alloys have made their niche as a major material of construction in the transportation industry because of their very high strength level to weight ratio. There are many properties and factors in addition to high strength to weight ratio, which affect the decision of the designers in selecting a new or improved materials for the various components and parts. Some of them are: high stiffness, fracture toughness, corrosion resistance, environmental capability, producibility,

machining and finishing qualities, material compatibility and product form availability.

For every weight % of lithium added to an aluminum alloy, the density is reduced by approximately 3 % and elastic modulus is increased by approximately 6 % , upto a 4 % of lithium addition[11]. It is this property which made Al-Li alloys as an alternative materials in addition to their other property advantages. The comparison of typical mechanical properties of 2XXX and 7XXX series aluminum alloys with the initially developed Al-Li alloy 2020 is given in Table 1. Table 2 indicates that the recently developed Al-Li alloys have the lowest densities among all other commercial wrought aluminum alloys. The average density of Al-Li alloy is found to be 2.557 g/cm³.

Aluminum alloys may not fully replace the steels for the entire structure of the automobile vehicles in the immediate future due to various reasons. As of today, based on the technology available, the cost of manufacturing of steel components is less than the components made out of Al alloy components. However, the usage is always in the increasing trend. When the cost of petroleum products overrides the cost of steel manufacturing, Al alloys will find their way as a market leader. That day is not very far. This is clearly evident from the fact that today's automobiles use more than 6 wt % of aluminum alloys structures in their construction. Fifteen years ago, this figure was only 2.5 wt %[12]. In the case of aerospace industries, the thrust is much higher for the usage of lightweight materials. In the present technology, 2XXX series and 7XXX series alloys are the major construction materials for aerospace structures. On the other hand, 2XXX series along with 5XXX and 6XXX series alloys are the major construction materials in automobile and naval structures.

Table 1. Mechanical Properties of Different Aluminum Alloys[3,13]

Alloy and Temper	Tensile Strength (MPa)	Yield Strength (MPa)	Elongation (%)	Shear Strength (MPa)
2020 - T6*	579	531	3	338
2024 - T86	517	490	6	310
7075 - T6	572	503	11	331
7079 - T6	538	469	14	310
7178 - T6	607	538	11	359
2090 - T83*	629	-	-	-
8090 - T8*	480	-	-	-

* Aluminum -Lithium Alloys

Table 2. Densities of Different Aluminum Alloys[3,14]

Alloy	Density (gm / cm ³)
99.99 wt % Al	2.70
1050	2.71
3103	2.73
5005	2.69
5154	2.69
2014	2.80
2024	2.77
2618	2.75
6101	2.70
6063	2.70
6082	2.70
7020	2.78
7075	2.80
2090*	2.57
2091*	2.55
8090*	2.55

* aluminum-lithium alloys

In the recent years, Al-Li alloys designated under 8XXX and 2XXX series have become important advanced structural materials for aerospace applications. The first commercially available Al-Li alloy developed was 2020, announced by ALCOA in 1958, for the use on the Navy RA-5C vigilante military aircraft[15]. Since then, numerous other alloys have been developed in various forms. However, several property and processing problems were faced. The concern about the low fracture toughness made the manufacturers to terminate the commercial exploitation of Al-Li alloys in late 1960's. In the mid 1970's , the Navy , the Naval Air Systems Command (NAVAIR) in particular, launched extensive R & D efforts on Al-Li alloys to meet the demands of high performance future aircrafts[16]. It planned, executed and coordinated the program involving cooperation among primary producers, fabricators, users and universities. At the same time, major manufacturers like ALCOA, restarted the efforts of developing a commercially available Al-Li alloys containing 2 to 3 wt % lithium.

The main disadvantage of these Al-Li alloys are lower ductility and toughness and poor corrosion resistance. These problems have been reduced and improvements have been achieved by recent processing methodology such as vacuum refining [17].

2.1. Alloy Development

The overall strategy of Al-Li alloy development is aimed at the replacement of 2XXX and 7XXX series alloys. These two class of alloys are the major construction materials with superior strength and corrosion properties. The main properties of these alloys that are being targeted at replacing with aluminum-lithium alloys are shown in Table 3.

Table 3. Design Properties of Alloys Considered for Replacement by Al-Li Alloys[3,18]

Al - Li Alloys	Replacement for	Design Criteria
2090 - T83	7075 - T6	High strength
2090 - T84	7075 - T76	High strength and Toughness
2090 - T81	7075 - T651	High strength
2090 - T86	7075 - T6511	High strength
2091 - T84	2024 - T3	Damage tolerance
8090 - T852	7075 - T73	Medium Strength, Stress corrosion resistance

The concept of damage tolerance means the ability of the alloy to prevent the formation and growth of cracks to a critical size and in the critical cases, ability to suppress the early stages of crack initiation. Fracture toughness is a measure of damage tolerance of the material. High fracture toughness can be achieved, if by some means stored energy can be released as plastic deformation rather than by cracking. A low yield stress will allow the generation of large plastic zone and the early onset of plastic deformation with applied strain. Therefore, a low ratio of yield strength to ultimate tensile strength will increase the damage tolerance of the alloy. Another factor need to be considered is fatigue crack initiation. In general, stronger the material, higher the intrinsic fatigue strength. Therefore, alloys precipitation hardened to their highest strength level perform better. The properties of higher strength level and a low ratio of yield strength and ultimate tensile strength are both easily achieved in 2091 T84 alloy similar to 2024 T3 alloy.

A series of tests were conducted at Naval Air Development Center to study the corrosion behavior of aluminum-lithium alloys[15]. In general, corrosion tests by salt spray plus sulfur dioxide conducted on 7075 alloys are in good agreement with the real time corrosion results. But in the case of aluminum-lithium alloys conflicting results were obtained. Though, very poor rating was obtained on the laboratory tests, the real time atmospheric results of 8090 alloys were found to be superior to the 7075 alloy. The surface appearance and rating of actual exposure tests on 8090 alloy are the same as that of 7075 alloy. These tests proved that comparable corrosion resistance properties can be achieved in aluminum-lithium alloys.

Table 4. Nominal Compositions of Different Aluminum-Lithium Alloys[3]

Elements	Alloys (wt %)				
	2090	2091	8090	2095	Al-905XL
Si	0.10	0.20	0.20	0.12	-
Fe	0.12	0.30	0.30	0.15	-
Cu	2.4-3.0	1.8-2.5	1.0-1.6	3.9-4.6	-
Mn	0.5	1.10	0.10	0.10	-
Mg	0.25	1.1-1.9	0.6-1.3	0.25-0.6	4.0
Cr	0.05	0.10	0.10	-	-
Zn	0.10	0.25	0.25	0.25	-
Li	1.9-2.6	1.7-2.3	2.2-2.7	1.0-1.6	1.3
Zr	0.08-0.15	0.04-0.16	0.04-0.16	0.04-0.18	-
Ti	0.15	0.10	0.10	0.10	-
Aluminum	Remainder	Remainder	Remainder	Remainder	Remainder

High strength aluminum alloys are used in their peak strength conditions for critical applications that require high inplane strength sacrificing the short transverse compressive strengths. In addition to this, high modulus are required to resist buckling and stability during bending. aluminum-lithium alloy 2090 provides very high specific modulus with a very high specific strength. These properties achieved in the currently used 7075 alloy can be conveniently attained in the 2090 alloy. The typical compositions of all the three commercially available aluminum-lithium alloys 2090, 2091 and 8090 from ALCOA and other two developmental alloys are shown in Table 4.

2.2. Processing Methods

Despite the unique advantages of Al-Li alloys, the full commercial utilization of these alloys has fallen short of initial expectations. This is partly due to the lower ductility and toughness of these alloys, when compared to the 7XXX alloys. The two major reasons that result in this property loss are[17]: (1) strain localization problem, and (2) liquid metal embrittlement by alkali metal impurities . The former problem can be fixed by changing the deformation mode associated with dislocation looping or bypassing the precipitates which is easily accomplished by over aging in age-hardenable alloys. The latter problem is purely associated with processing in which the impurities come from the lithium alloying additions. The reduction of alkali impurities to a very low level is very difficult in the current ingot metallurgy process route. Other processes such as powder metallurgy and vacuum refining are being tried to alleviate this problem. From this point of view, the new in-situ method of processing Al-Li alloys in a molten salt media, investigated in this research work virtually eliminates this impurities problem.

Here, lithium compounds are used, instead of pure metallic lithium, as lithium sources. Even if some impurities are present in the compound, they all will be trapped in the molten salt media which acts as flux to eliminate these impurities.

In addition to this there are problems associated with lithium metal itself. It is extremely reactive and thereby complicates the alloy production. Melts containing lithium in excess of 1.5 wt % explode violently in contact with moisture or water[16]. Therefore, direct chill casting of these alloys by ingot metallurgy route requires special equipments and precautions. Another problem area that has been addressed is the ingot qualities. Al-Li alloys have more affinity for gases like H_2 , O_2 , and N_2 from atmosphere. One major problem resulting from these gases, especially from hydrogen pickup, is porosity in ingots. These porosities lead to blisters and flakes in the wrought products made from ingots. In this new process, the molten salt electrolyte acts as a blanket and there is no direct contact between the alloy formed and the atmosphere. Hence, it eliminates the pick up of gases from atmosphere.

The cost of pure lithium metal per pound is very much higher when compared to the cost of the lithium compounds. The energy cost involved in this new process need to be added to the overall process and raw material costs. Approximate estimates indicate that, even after adding the energy costs, the process would be less expensive when compared to the processes utilizing the pure lithium metal for alloy production. However, the actual estimation of processing costs need to be done. Thus, the new process investigated in this research offers a viable technological alternative to other processes, due to the above mentioned factors.

2.3. Solubility of Oxides and Chlorides in Halide Melts

The process of obtaining a metal from its oxides by electrolysis was pioneered by the Hall-Herault process of aluminum electrowinning. Since then, it has been well established that in halide electrolytes, only the dissolved oxides are available for the dissociation at the electrode to release the metal during electrolysis. Therefore, the solubility of these metallic oxides in the electrolytes is an important parameter which determines the economical and technical viability of the molten salt electrolysis process. Halides are the major class of electrolytes used in molten salt electrolysis of metal and alloys. Among halides, the fluorides and chlorides are very commonly used electrolyte mediums due to their less hygroscopic and low melting point characteristics. Generally, chlorides have low melting points. However, fluorides are preferred over chlorides in many molten salt processes due to their higher electrical conductivity and higher solubility for oxides.

A number of studies have been carried out on the dissolution of alumina in cryolite and halide melts due to their commercial interest in primary aluminum production. Thonstad et.al.[19] studied the rates of dissolution of alumina and the formation of sludges from the undissolved alumina. It was concluded that rates are independent of oxides concentration below the saturation level. Winkhaus[20] studied the dissolution of different types of alumina in cryolite melts and found that the dissolution characteristics depend on the degree of calcination of the oxides. Haupin[21] analyzed the solubility of alumina in chloride melts and proposed a model for the reactions taking place during the dissolution of alumina. He found that the dissolved species to be AlOCl

and concluded that the solubility increased with cube root of activity of the component salt (AlCl_3) of the electrolyte. In recent years, attempts have been made to utilize the mixed fluoride-chloride to gain advantage over the properties of both the systems. The presence of fluorides in these melts increases the solubility of oxides in the electrolyte. Picard et.al.[22], studied the effect of NaF addition on the solubility of alumina in LiCl-KCl eutectic melt. The solubility product of γ and α alumina in the presence of NaF was determined to be $10^{-42.9}$ and $10^{-44.0}$. This is much higher than the solubility product $10^{-27.4}$ of alumina in the absence of fluoride ion.

High melting temperature oxides such as Al_2O_3 , Y_2O_3 , La_2O_3 etc., are used as core materials in the investment casting process of blades for high pressure turbine engines. In a study to explore the possibility of using molten salts as a dissolving media to remove the oxides after the casting process, Borom et.al.,[23] found that dissolution rate of alumina and other oxides are very high in Li_3AlF_6 system compared to pure LiF and NaF- CaF_2 eutectic. Wai and Blander[24] have used a proton activation technique to study the solubility of Al_2O_3 in LiCl-KCl eutectic mixture. The formation of the AlO^+ complex proposed theoretically was confirmed by this experimental studies. From these solubility studies they deduced a formation constant of 1.94×10^{22} (in mole fraction units) and a specific bond energy of 300 KJ mole for the couple.

All these studies on alumina increased the database and improved to a great extent of the understanding of alumina-halide systems. On the other hand, very limited work has been reported on the other oxide-halide, halide-halide, and halide-oxide systems. However, in recent years a number of these systems have been studied due to the increased interest in molten salts for the potential use in battery and fuel cells development and extraction of highly reactive and light metals and alloys.

Recently, Reddy and Kumar[25] studied the Y_2O_3 -LiF- YF_3 system and found that the dissolution of Y_2O_3 in LiF- YF_3 melts exhibited a negative deviation from Temkin ideal conditions. Suito and Gaskell[26] reported the depression of freezing points of pure fluoride, MgF_2 , CaF_2 and BaF_2 by the addition of different oxides. They determined variation of the activities of fluorides with liquidus composition and showed that results are in good agreement with their proposed theoretical model. Shiyong et.al.,[27] analyzed the solubility of rare earth oxides, La_2O_3 , CeO_2 and Y_2O_3 in cryolite-alumina based melts and deduced the regression equations for the dissolution behavior as a function of temperature and cryolite-alumina ratio.

Seefurth and Sharma[28] developed and used an optical technique to study the solubility of Li_2S in LiCl-KCl electrolyte melts. They deduced linear regression equations for the solubilities as a function of temperature and found that it varied from 3.24×10^{-4} mole fraction at 689 K to 3.15×10^{-3} mole fraction at 815 K. In an effort for electrowinning aluminum from chloride melts, Ishikawa et.al.,[29] studied solubilities of divalent metal chlorides $MnCl_2$, $MgCl_2$, $CdCl_2$, and $CoCl_2$ in binary chloride melts $AlCl_3 + NaCl_2$ in the concentration range from 55 to 59 mole % $AlCl_3$ at 473 K. They

used a ampoule sampling technique and found that the solubilities of all chlorides increase with increase in the concentration of AlCl_3 . In another recent study, the solubilities of AgCl in molten NaCl-AlCl_3 and KCl-AlCl_3 were reported by Tumidajski et.al.[30]. They used an electromotive force technique similar to the procedure that was used in the present study to determine the solubilities of Li_2O and Li_2CO_3 . They studied the solubility of AgCl at several solvent compositions and temperatures and found that it varied from 6.85×10^{-3} mole fraction to 1.25×10^{-2} mole fraction of AgCl .

The literature data collected on the solubilities of several oxides and chlorides in halide systems are given in Table 5 and Table 6 respectively. The reported solubility values of several compounds used for electrochemical processing of metals indicated that a minimum of 2 wt % of lithium oxide and lithium carbonate are required for the process to be feasible and successful deposition of lithium into aluminum to form Al-Li alloy.

2.4. Electrochemical Production of Metals and Alloys from Halide Melts

Eletrowinning and deposition from molten salt medium is a well established process route for the extraction and synthesis of light, reactive and refractory metals and alloys. After the Hall-Herault process became commercial success, a number of investigators tried to obtain various metals and alloys from different molten salt electrolyte systems.

Table 5. Solubilities of Various Oxides in Fluoride Electrolytes

Oxide	Electrolyte	Temp. (K)	Oxide Solubility (wt%)	X_{AxBy}	$\ln X_{AxBy}$	Ref.
Y_2O_3	80LiF-20YF ₃	1273	-	0.0065	-5.036	27
	50LiF-50YF ₃	1273	-	0.0211	-3.859	
Nd_2O_3	90NdF ₃ -10LiF	1373	2.0	0.0071	-4.948	31
	80NdF ₃ -20LiF	1373	2.0	0.0051	-5.279	
UO_2	40UF ₄ -57BaF ₂ -3LiF	1523	4.0	0.026	-3.650	32
	40UF ₄ -45BaF ₂ -15CaF ₂	1523	3.8	0.0238	-3.738	
CeO_2	63CeF ₃ -16BaF ₂ -21LiF	1073	1.4	0.007	-4.962	32
	63CeF ₃ -16BaF ₂ -21LiF	1123	2.1	0.010	-4.605	
La_2O_3	70LaF ₃ -10BaF ₂ -20LiF	1223	2.3	0.0052	-5.259	32
	84LaF ₃ -16LiF	1223	2.6	0.0076	-4.880	
SnO_2	55NaF-25AlF ₃ -5CaF ₂ -5Al ₂ O ₃	1223	1.2	0.0046	-5.382	33
	55NaF-25AlF ₃ -5CaF ₂ -5Al ₂ O ₃	1273	2.3	0.0088	-4.733	

Table 6. Solubilities of Various Chlorides in Chloride Electrolytes

Chloride	Electrolyte	Temp. (K)	$X_{A_xB_y}$	$\ln X_{A_xB_y}$	Ref.
CoCl ₂	55AlCl ₃ -45NaCl	473	5.263×10^{-3}	-5.247	29
	59AlCl ₃ -41NaCl	473	0.0184	-3.995	
CdCl ₂	55AlCl ₃ -45NaCl	473	0.0276	-3.590	29
	59AlCl ₃ -41NaCl	473	0.0684	-2.682	
MgCl ₂	55AlCl ₃ -45NaCl	473	0.0211	-3.859	29
	59AlCl ₃ -41NaCl	473	0.0421	-3.168	
AgCl	50AlCl ₃ -50KCl	534	5.020×10^{-3}	-5.294	30
	50AlCl ₃ -50KCl	583	6.850×10^{-3}	-4.984	
CoCl ₂	55AlCl ₃ -45NaCl	448	5.700×10^{-3}	-5.163	34
	60AlCl ₃ -40NaCl	448	2.000×10^{-3}	-6.215	
FeCl ₂	50AlCl ₃ -50NaCl	448	3.790×10^{-3}	-5.575	35
	50AlCl ₃ -50NaCl	528	2.190×10^{-3}	-6.124	

Several reports were published[31,36-41] on the production of rare earth, reactive and radioactive metals such as Dy, Gd, La, Ce, Nd, Sm, Pr, Y, mischmetal and uranium. The electrolyte mixtures used in most cases were made of rare earth fluoride and lithium fluoride (RF_3 -LiF), containing oxides as a feed material. 'R' represents the respective fluoride of the metal to be extracted. Current efficiencies in the range of 25-80 % were achieved in various processes. The lower efficiencies observed in certain cases were mainly due to: (1) higher reactivity of metal with the electrolyte; (2) higher temperature of operation of the cell; (3) the stability of ions in the form of salts. Morrice et.al.,[36] reported successful electrowinning of high purity cerium and mischmetal from the electrolyte CeF_3 -LiF- BaF_2 . At a later investigation[31] on the electrowinning of rare earth metals, very low current efficiencies of about 20 % observed in the case of yttrium. Some of the other problems faced by the operation of the cell at high working temperatures were, higher reactivity of the metal with the electrolyte, carbon contamination from the electrodes, and volatility of the electrolytes used. For some rare earth metals like, samarium, gadolinium, dysprosium electrowinning was possible only in the form of alloys. Especially, in the case of samarium, the stability of its divalent ion made it very difficult to obtain in the pure form. Recently, Dysinger and Murphy[42] reported the electrowinning of neodymium from a molten oxide-fluoride electrolyte. Neodymium metal was obtained by the electrolysis of Nd_2O_3 in the molten NdF_3 -LiF- CaF_2 electrolyte. Neodymium metal with a purity as high as 99.8 % was recovered for current efficiencies in the range of 50-60 % with a current density up to 0.30 A/cm^2 .

One way reducing the temperature of operation during molten salt electrolysis of metals is by forming low melting alloys. A number of investigators reported the successful utilization of this technique. The strategy involved in the production of rare earth and reactive alloys by electrolysis using this method is: (1) electrodepositing the metal into a liquid cathode pool by alloying with a lower melting metal such as zinc, magnesium and aluminum; (2) electrodepositing the metal on to another solid metal cathode to form a liquid alloy; (3) codepositing the metals from mixtures of respective oxides.

One of the very early attempt was for the production of magnesium-lithium alloys from lithium chloride electrolyte by Smolinski et.al.[43,44]. They studied the relation between sodium contamination in electrolyte and alloy product and successfully produced Mg-Li alloys with a sodium content of less than 0.1 wt %. Aamland et.al.[37] studied the effect of parameters such as current density, temperature and electrolyte density on the preparation of magnesium-yttrium alloys by dissolving Y_2O_3 in YF_3 -LiF electrolyte. Alloys containing upto 55 wt % of yttrium were prepared at cathode current efficiencies of upto 60 %. The maximum current efficiency was obtained in the temperature range of 1063 K to 1173 K at a cathode current density of less than 2 A/cm^2 . Kirby et.al.,[45] investigated the preparation of beryllium-copper alloys by depositing beryllium on the solid copper cathodes. The beryllium was obtained by electrolysis beryllium oxide in LiF-BeF₂ electrolyte. They achieved current efficiencies in the range of 65-90 %. The current densities were in the range of $1\text{-}2.5 \text{ A/cm}^2$ in producing a 3-4 wt% beryllium alloy.

Chamber and Murphy[46], reported the electrowinning of neodymium metal from NdCl_3 into a molten cathode consisting of binary alloys Mg-Zn or Mg-Cd. The electrolyte used was $\text{NdCl}_3\text{-KCl}$ with 50-50 mole %. Current efficiency was 90 % for Mg-Zn cathode and 80 % for Mg-Cd alloy cathode. Current density were in the range of 0.22 A/cm^2 to 1.30 A/cm^2 . Neodymium metal and alloy cathode were separated later by vacuum distillation and the purity of recovered metal was above 99.9 %.

1.2. Experimental Studies

The solubility of lithium oxide (Li_2O) and lithium carbonate (Li_2CO_3) were investigated at various temperatures ranging from 943 K to 1133 K in LiF-CaF_2 electrolytes. The feasibility of using argon as an inert electrolyte, and the electrolyte saturated with Li_2CO_3 were determined. The experimental techniques used and results obtained are described in the following sections.

3. SOLUBILITY OF LITHIUM OXIDE AND LITHIUM CARBONATE IN LiF-CaF₂ MELTS

3.1. Theoretical Background

The Phase diagram of the aluminum-lithium alloy system is shown Figure 1. It contains an eutectic existing at 8.2 wt% of lithium (25.8 atom%) with a melting point of 873 K[47,48]. Liquid compositions exist between pure aluminum and the alloy (87 wt% Al and 13 wt% Li) at 933 K, the melting point temperature of aluminum. The maximum solubility of lithium in aluminum at this temperature is about 4.0 wt% and reduced as the temperature is lowered which facilitates the precipitation hardening process in this system. The phase diagram of the LiF-CaF₂ salt system is shown in Figure 2. This has an eutectic point at 57.8 wt% (80.5 mole%) of LiF and 42.2 wt% (19.5 mole%) of CaF₂ with a melting temperature of 1042 K[49]. Therefore, usable aluminum-lithium alloy compositions can be obtained by the electrochemical dissociation of lithium compounds at temperatures more than 1042 K which is very well above the eutectic temperature 933 K of the Al-Li alloy.

3.2. Experimental Studies

The solubility of lithium oxide (Li₂O) and lithium carbonate (Li₂CO₃) were investigated at various temperatures ranging from 1063 K to 1133 K in LiF-CaF₂ electrolyte. The liquidus freezing temperatures of the bare electrolyte, and the electrolyte saturated with Li₂CO₃ were determined. The experimental techniques used and results obtained are analyzed in the following sections.

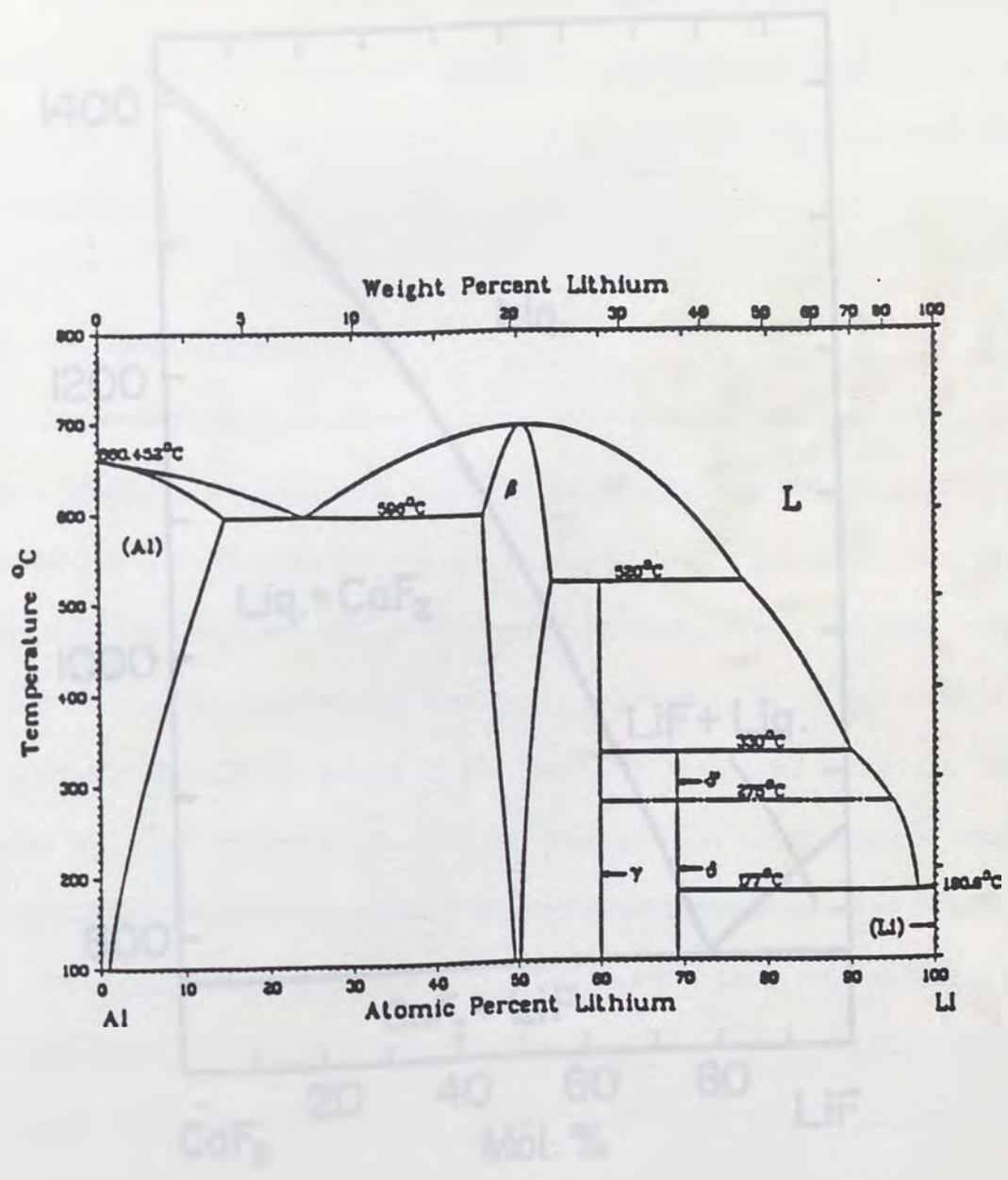


Figure 1. Aluminum-Lithium Phase Diagram

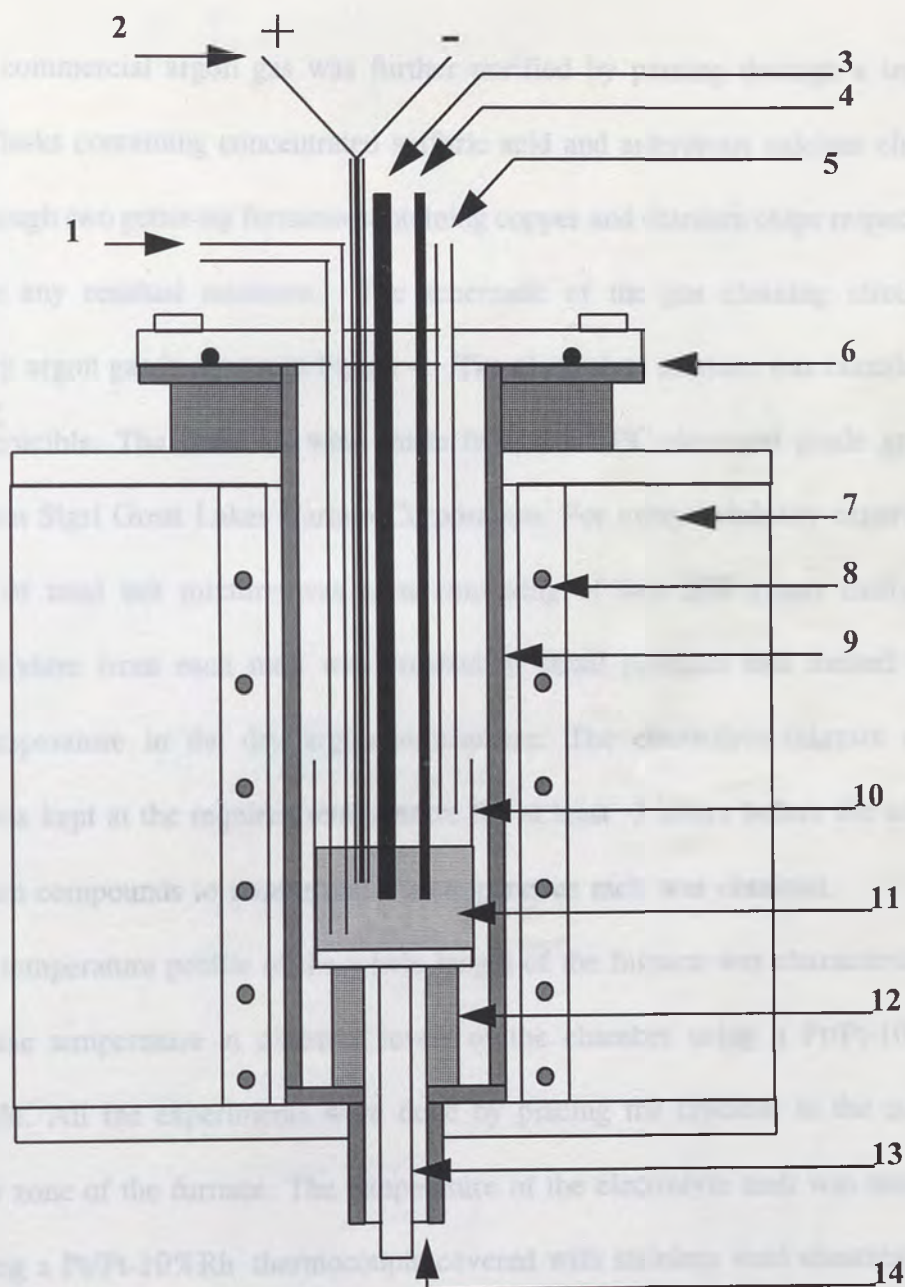
3.2.1. Materials Used

Calcium fluoride of 99.9 % purity from Aldrich Chemical Co., Lithium fluoride of 99.9 % purity from Foote Mineral Co., Lithium oxide of 99.5 % purity from Cerac, Inc., and Lithium carbonate of 99.8 % purity from Fisher Scientific were used in the studies.

3.2.2. Experimental Procedure

The experiments on the solubility studies were carried out in a electrically heated furnace chamber. The experimental setup consisted of a 11.5 cm diameter cylindrical superalloy chamber. The chamber was closed by flange on the top with a vacuum tight O-ring seal. The flange had ports to the chamber for inert gas inlet and outlet, oxide additions, evacuation, thermocouple and electrode insertion. The cooling water was circulated near the neck on the top of the chamber to protect the O-ring seal. The chamber was heated by a split type cylindrical heating coil of 14 cm diameter wound with kanthal wire. A schematic outline of the experimental setup is shown in Figure 3.

The established phase diagram of LiF-CaF_2 has an eutectic point at 1042 K as mentioned earlier. The electrolyte composition at this eutectic point was selected for all the studies. The calcium fluoride and lithium fluoride were weighed and mixed in stoichiometric proportions to have the eutectic composition. A mixture of total weight 200 grams was used in each melting. The LiF-CaF_2 mixture weighed in the required proportion was dried in a continuous vacuum at 423 K for 4 hours and melted at 1123 K in a dry argon atmosphere for 2 hours.

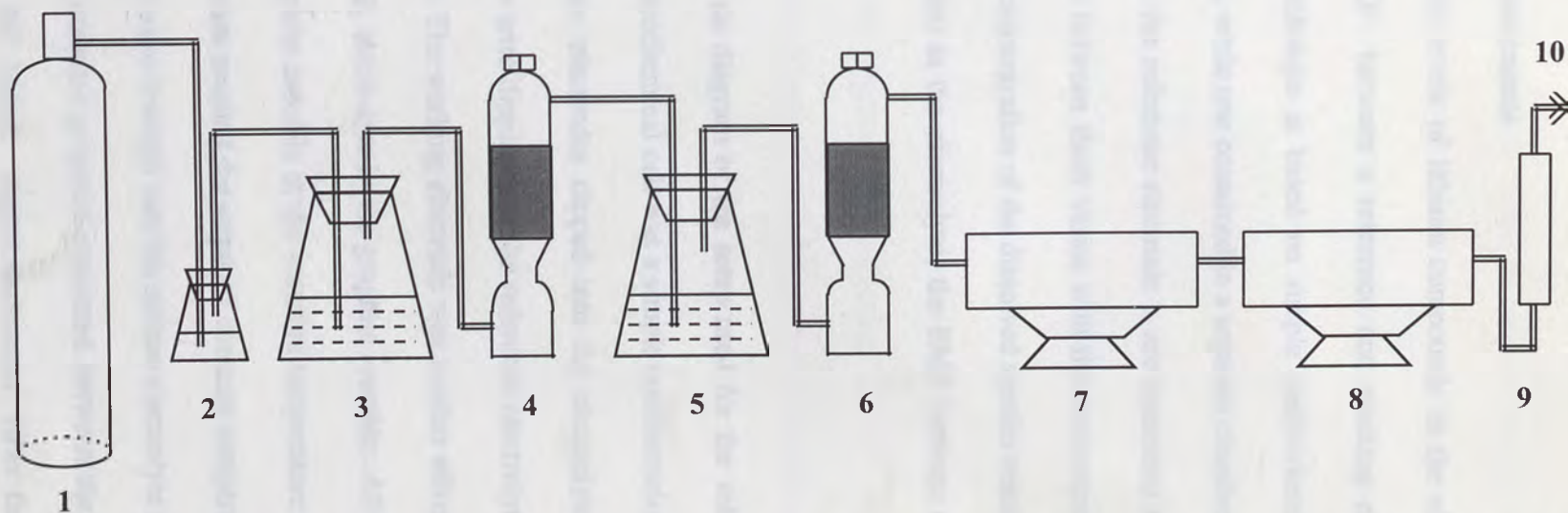


- | | |
|------------------------------|----------------------------|
| 1. Gases inlet | 8. Kanthal heating element |
| 2. Thermocouple | 9. Superalloy chamber |
| 3. Anode | 10. Graphite crucible |
| 4. Reference electrode | 11. Electrolyte |
| 5. Oxide additions/ Offgases | 12. Bottom support brick |
| 6. O-ring seal | 13. Cathode connection |
| 7. Thermal insulating wool | 14. To vacuum pump |

Figure 3. Sectional view of the experimental setup

The commercial argon gas was further purified by passing through a train of absorption flasks containing concentrated sulfuric acid and anhydrous calcium chloride and then through two gettering furnaces containing copper and titanium chips respectively to eliminate any residual moisture. The schematic of the gas cleaning circuit for obtaining dry argon gas is shown in Figure 4. The electrolyte mixture was contained in a graphite crucible. The crucibles were made from the HPC electrical grade graphite obtained from Sigri Great Lakes Carbon Corporation. For every solubility experiment, 400 grams of total salt mixture was used consisting of two 200 grams melts. The solidified mixture from each melt was crushed to small particles and melted at the required temperature in the dry argon atmosphere. The electrolyte mixture during remelting was kept at the required temperature for at least 3 hours before the addition of the lithium compounds to ensure that a homogeneous melt was obtained.

The temperature profile of the whole length of the furnace was characterized by measuring the temperature at different levels of the chamber using a Pt/Pt-10% Rh thermocouple. All the experiments were done by placing the crucible in the constant temperature zone of the furnace. The temperature of the electrolyte melt was measured by immersing a Pt/Pt-10%Rh thermocouple covered with stainless steel sheathing. The thermocouple and the SS protection tube were obtained from Omega Corporation. The temperature was read from a Digital temperature indicator connected to the thermocouple. The calibrated temperature indicator was Trendicator 400 from Doric Inc., with a resolution of ± 1 K.



- | | |
|--|-------------------------------------|
| 1. Argon gas cylinder | 2, 4, 6. Calcium chloride |
| 3, 5. Conc. H ₂ SO ₄ | 7. Getter furnace with copper chips |
| 8. Getter furnace with titanium chips | 9. Flowmeter |
| 10. To furnace gas inlet | |

Figure 4. Schematic diagram of argon gas cleaning setup

3.2.3. EMF Measurements

The solubility levels of lithium compounds in the electrolyte were studied by measuring the EMF between a reference and working electrode immersed in the electrolyte. This technique is based on simple electrochemical principle. When two different electrodes, while one contained in a separate chamber to avoid the mass transfer (in our case it was the reference electrode), are immersed in the same electrolyte, the potential difference between them varies with the concentration of the dissolved ionic species. When the concentration of the dissolved species reaches the maximum solubility limit (i.e., saturation) in the electrolyte, the EMF between the electrodes will attain a stable value.

The schematic diagram of the setup used for the solubility studies is shown in Figure 5. The electrochemical cell was a simple concentration cell. It consisted of silver metal wire indicator electrodes dipped into the electrolyte solutions. The reference electrode is a silver wire dipping into the reference electrolyte AgF-LiF-CaF_2 contained in an alumina tube. The working electrode was another silver wire dipping directly into the molten LiF-CaF_2 electrolyte in the graphite crucible. All the experiments were done by placing the graphite crucible at the constant temperature zone of the furnace. After the electrolyte mixture reached the required constant temperature, the reference and the working electrodes were lowered into the molten electrolyte and allowed to remain until the cell reached a constant potential measured between the electrodes. The EMF was measured using a HP 3466A digital multimeter. After the equilibrium was reached,

the lithium compound (lithium oxide or lithium carbonate) was added in weighed quantities to the electrolyte and the melt was stirred by purging argon gas through the melt and voltages were measured after each addition. Electromotive forces were allowed to stabilize for every addition and these stable voltages were recorded. Argon purging stopped and the tube was raised above the electrolyte and the melt was allowed to settle down before recording each voltage reading. Generally, emf was stable within 30 minutes of material addition. The quantity of the lithium compound added until the point beyond which the EMF became stable was the solubility level of the compound in the LiF-CaF₂ electrolyte at the given temperature.

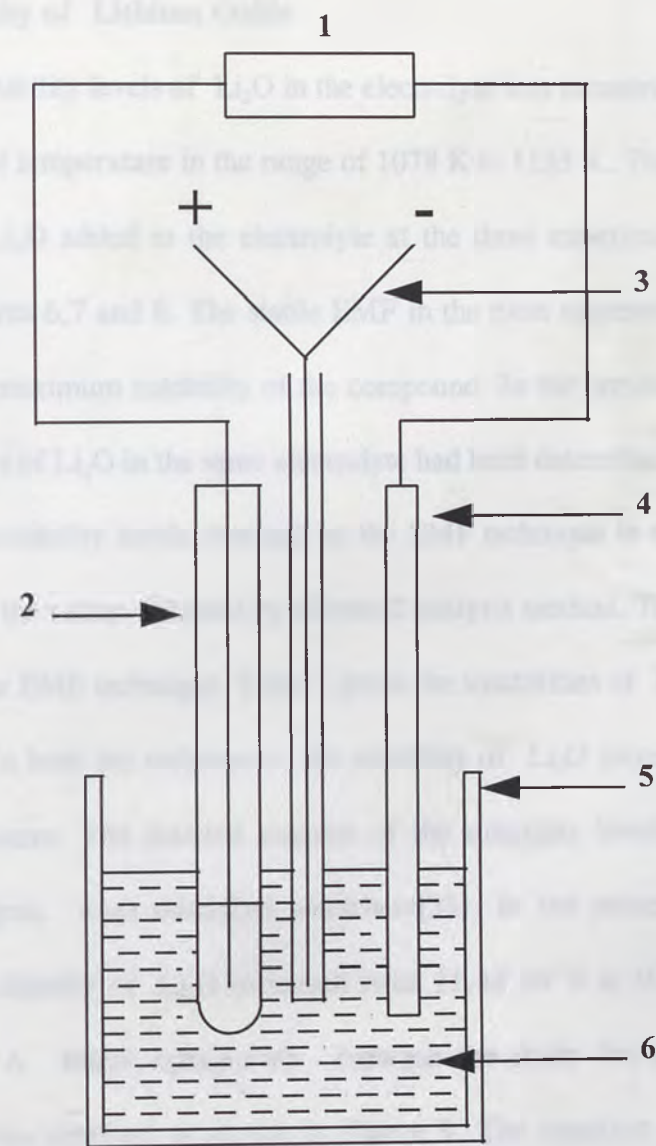
3.2.4. Procedure for Liquidus Temperatures

The efficiency of any electrolysis partially depends on the temperature at which the process is carried out. Therefore, to determine the optimum temperature for the electrolysis of Li₂CO₃ in LiF-CaF₂ electrolyte, the liquidus temperature of LiF-CaF₂+Li₂CO₃ (saturated) melt was determined by the cooling curve method. The same experimental setup described earlier as shown in Figure 3 was used. Excess amount of Li₂CO₃ was added to the eutectic mixture of LiF-CaF₂ and the melt was held at 1123 K for 6 hours after the addition of Li₂CO₃. Temperature was measured using Pt/Pt-10% Rh thermocouple enclosed in a thin SS protection sheath. The melt was cooled in the furnace argon atmosphere. Two sets of heating and cooling cycles were performed and cooling curves were determined. Similar cooling curves were also obtained for pure electrolyte LiF-CaF₂ without any lithium compounds added.

3.3. RESULTS AND DISCUSSION

3.3.1. Solubility of Lanthan Oxide

The solubility of La_2O_3 in the electrolyte was measured by the EMF method as a function of temperature in the range of 1078 K to 1133 K. The change of EMF with the wt% of La_2O_3 added to the electrolyte at the three experimental temperatures are shown in Figures 5, 7 and 8. The EMF in the peak represents the maximum level and gives the maximum solubility of the compound. In the present study [20,21] the solubility levels of La_2O_3 in the electrolyte had been determined by chemical analysis method. The solubility levels obtained by the EMF method in the present study agree very well with the results obtained by the chemical analysis method. This confirms the results obtained by the EMF method. The solubility levels of La_2O_3 measured by both the methods. It has been observed that the solubility levels of La_2O_3 increased with the increase in the temperature. The solubility levels of La_2O_3 obtained by chemical analysis in the present study by the EMF method, are shown in Figures 5, 7 and 8. The solubility levels of La_2O_3 and the temperature dependence of the EMF are shown in Figures 5, 7 and 8.



- | | |
|-----------------|------------------------|
| 1. Multimeter | 2. Reference electrode |
| 3. Thermocouple | 4. Working electrode |
| 5. Crucible | 6. Electrolyte |

Figure 5. Schematic diagram of the EMF measurement setup

3.3. RESULTS AND DISCUSSION

3.3.1. Solubility of Lithium Oxide

The solubility levels of Li_2O in the electrolyte was measured by the EMF method as a function of temperature in the range of 1078 K to 1133 K. The change of EMF with the wt% of Li_2O added to the electrolyte at the three experimental temperatures are shown in Figures 6,7 and 8. The stable EMF in the plots represents the saturation level and gives the maximum solubility of the compound. In the previous studies [50,51] the solubility levels of Li_2O in the same electrolyte had been determined by chemical analysis method. The solubility levels obtained by the EMF technique in the present study agree very well with the values obtained by chemical analysis method. This confirms the results obtained by the EMF technique. Table 1 gives the solubilities of Li_2O measured by both the methods. In both the techniques, the solubility of Li_2O increased with the increase in the temperature. The detailed analysis of the solubility levels of Li_2O obtained by chemical analysis were described elsewhere[51]. In the present study by the EMF method, the solubility of Li_2O increased from 11.42 wt % at 1078 K to 14.77 wt % at 1133 K. A linear relationship between the mole fraction of Li_2O and the temperature was obtained as shown in Figure 9. The equation obtained by the linear regression method is given below:

$$\ln X_{\text{Li}_2\text{O}} = 3.217 - \frac{5622.0}{T} \quad (1)$$

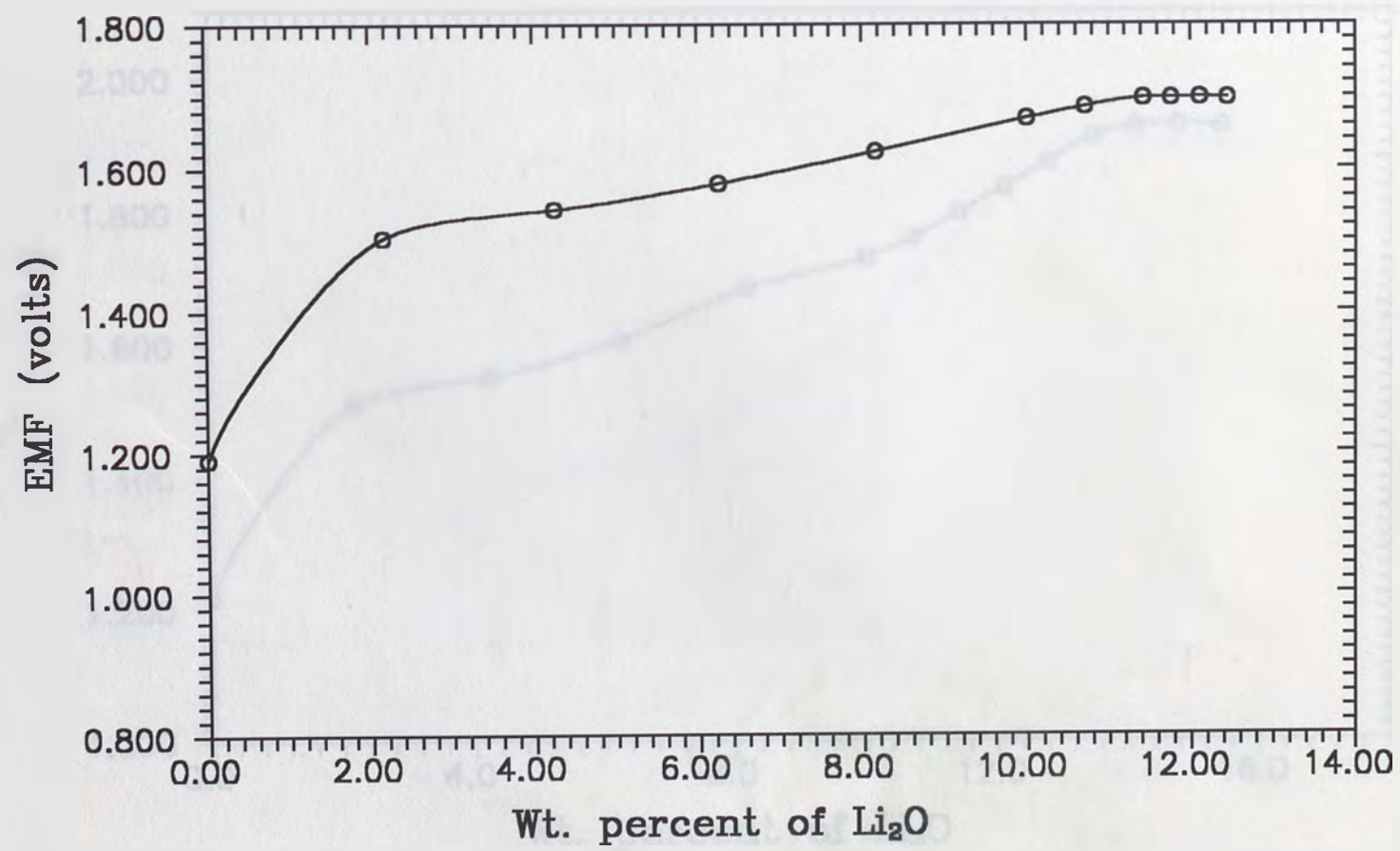


Figure 6. EMF Vs Wt. percent of Li_2O dissolved at 1078 K

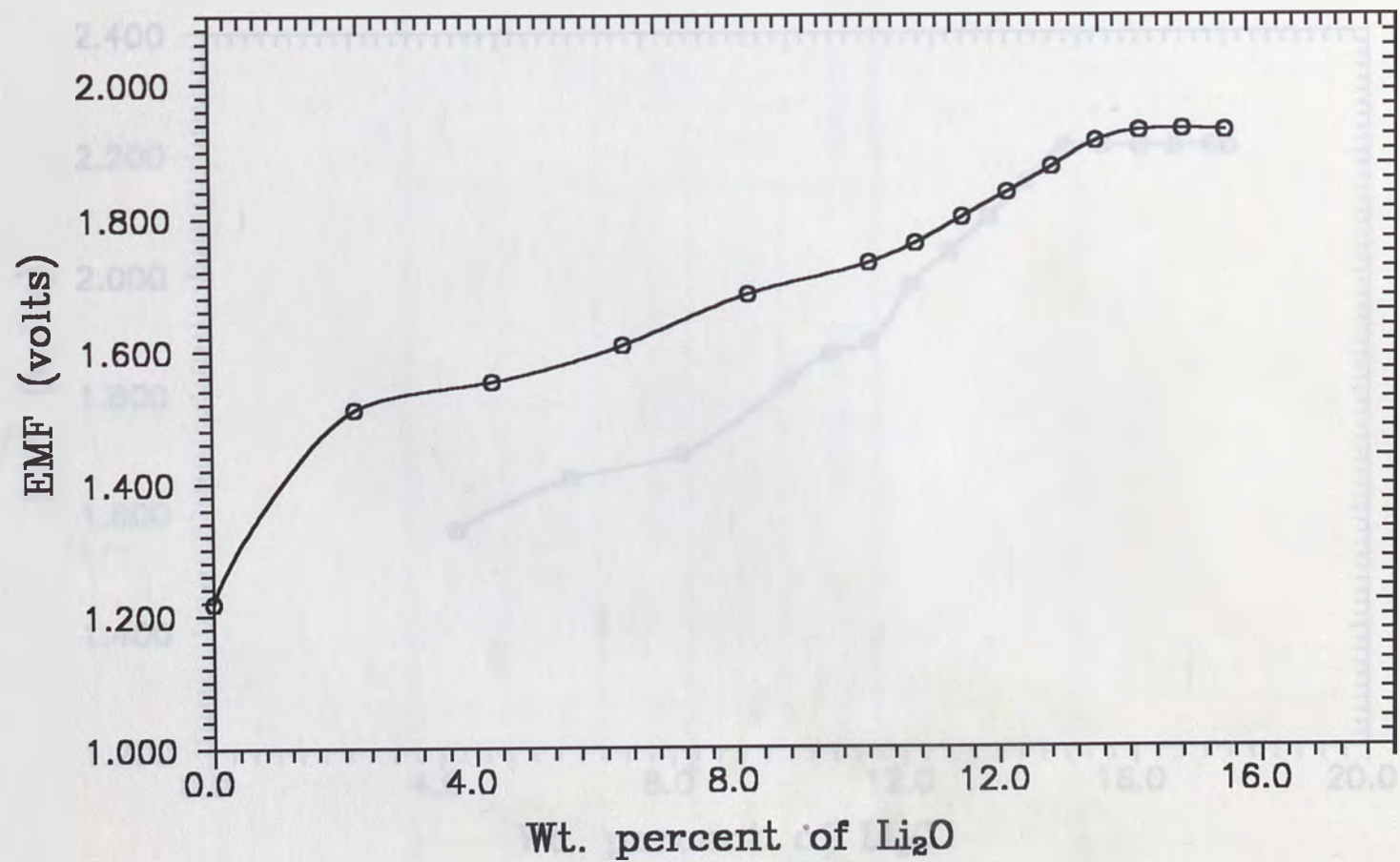


Figure 7. EMF Vs Wt. percent of Li_2O dissolved at 1113 K

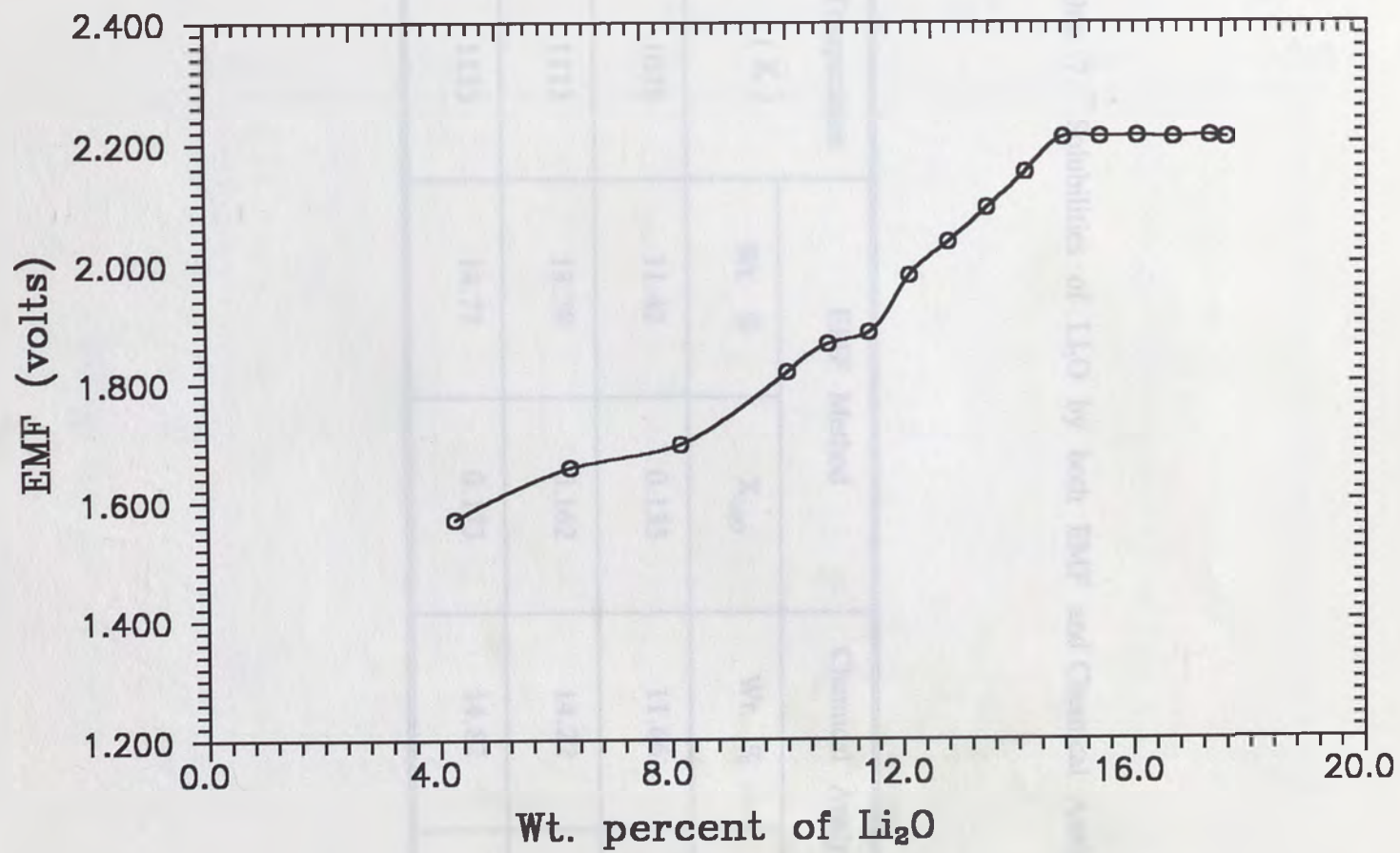


Figure 8. EMF Vs Wt. percent of Li_2O dissolved at 1133 K

Table 7. Solubilities of Li₂O by both EMF and Chemical Analysis Methods

Temperature (K)	EMF Method		Chemical Analysis Method	
	Wt. %	X _{Li₂O}	Wt. %	X _{Li₂O}
1078	11.42	0.135	11.66	0.159
1113	13.79	0.162	14.22	0.187
1133	14.77	0.173	14.82	0.193

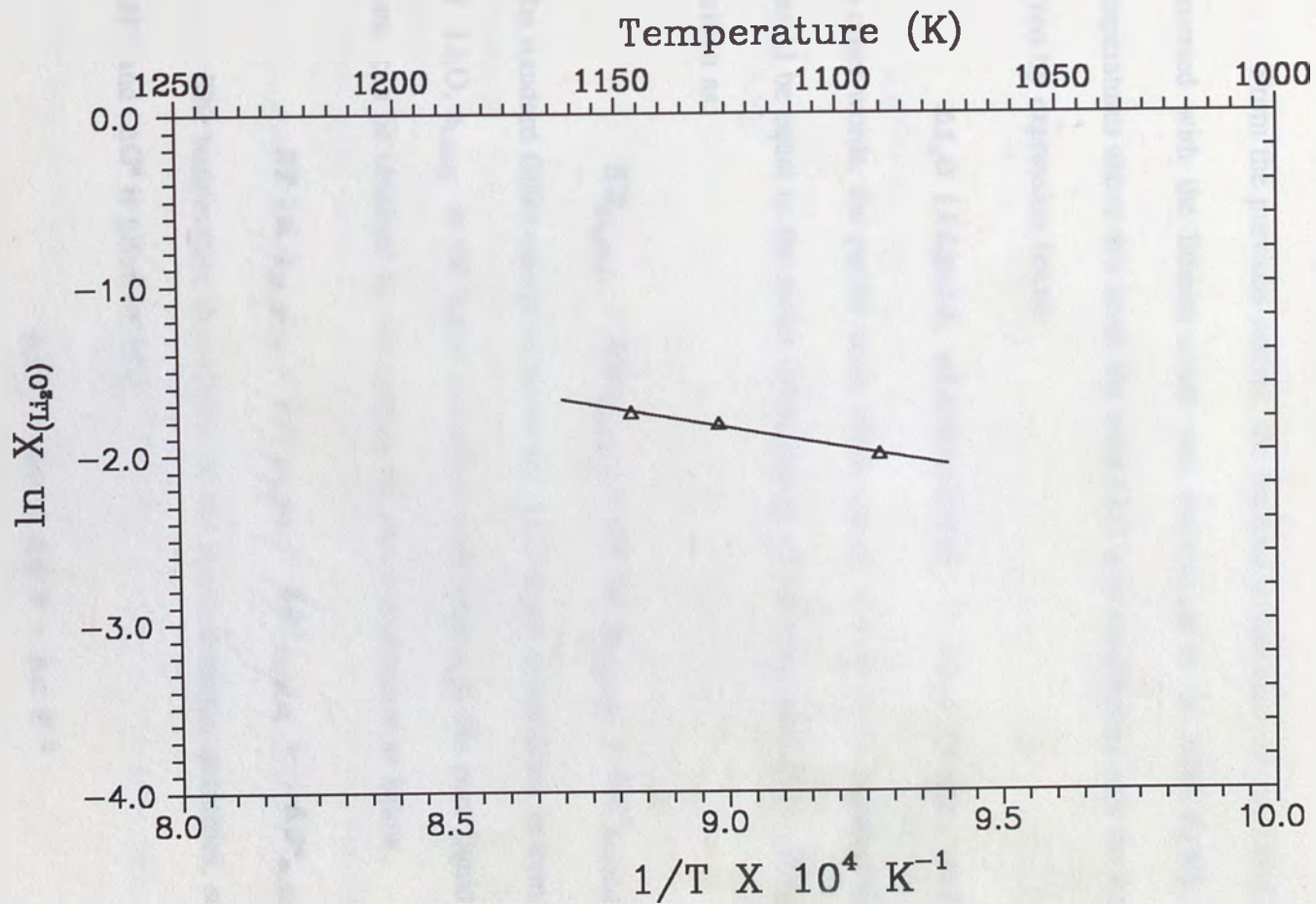
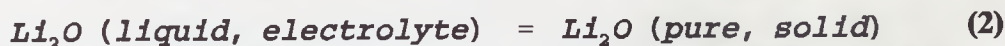


Figure 9. Variation of $\ln X_{Li_2O}$ with temperature

3.3.2. Activity of Li_2O in the Melt

From the previous studies, the liquidus temperature of the LiF-CaF_2 electrolyte saturated with the lithium oxide was determined to be 1004 K [50]. Therefore, at temperatures above this level, the solid Li_2O is in equilibrium with the liquid electrolyte given by expression below:



In other words, the partial molar Gibbs energy of Li_2O in the liquid electrolyte $\Delta G_{\text{Li}_2\text{O(l)}}$ should be equal to the molar Gibbs energy of the pure solid Li_2O $\Delta G_{\text{Li}_2\text{O(s)}^\circ$. It can be written as:

$$\overline{\Delta G}_{\text{Li}_2\text{O(l)}} = \Delta G_{\text{Li}_2\text{O(l)}^\circ} + RT \ln a_{\text{Li}_2\text{O(l)}} = \Delta G_{\text{Li}_2\text{O(s)}^\circ} \quad (3)$$

The standard Gibbs energy of fusion for Li_2O at any temperature in terms of the activity of Li_2O , $a_{\text{Li}_2\text{O(l)}}$ in the liquid electrolyte with respect to the pure liquid Li_2O standard state, can be obtained by rearranging the above expression as below.

$$RT \ln a_{\text{Li}_2\text{O(l)}} = \Delta G_{\text{Li}_2\text{O(s)}^\circ} - \Delta G_{\text{Li}_2\text{O(l)}^\circ} = -\Delta G_{m, \text{Li}_2\text{O}}^\circ \quad (4)$$

The temperature dependence of the thermodynamic quantities, such as, ΔC_p° , ΔH° and ΔG° is given by: [52]

$$\Delta C_p^\circ = \Delta a + \Delta b T + \Delta c T^{-2} \quad (5)$$

$$\Delta H^\circ = \Delta H_0 + \Delta a T + \frac{1}{2} \Delta b T^2 - \frac{\Delta c}{T} \quad (6)$$

$$\Delta G^\circ = \Delta H_0 - \Delta aT \ln T - \frac{1}{2} \Delta bT^2 - \frac{\Delta c}{2T} + IT \quad (7)$$

The procedure for the determination of the constants a , b and c and the integration constants ΔH_0 and I are described elsewhere[51] and the final expressions for ΔC_p° , ΔH° and ΔG° are given by:

$$\Delta C_p^\circ = 25.907 - 12.528 \times 10^{-3}T + 18.822 \times 10^5 T^{-2} \quad (8)$$

$$\Delta H^\circ = 33,127 + 25.907T - 6.264 \times 10^{-3}T^2 - \frac{18.822 \times 10^5}{T} \quad (9)$$

$$\Delta G_{m, Li_2O}^\circ = 33,127 - 25.907 T \ln T + 6.264 \times 10^{-3}T^2 - \frac{9.411 \times 10^5}{T} + 165.556T \quad (10)$$

Combining equations (4) and (10), the activities of Li_2O , at the experimental temperatures, were calculated. Using this activities and the mole fractions of the dissolved Li_2O at these temperatures, obtained from the experimental data on solubility measurements, the activity coefficients of Li_2O were also determined. The activities and activity coefficients of Li_2O calculated are given in Table 8. The activities and activity coefficients of CeO_2 in fluoride melts calculated using the same procedure described above were published elsewhere[53].

The measurements reported in this paper are consistent with these values. They are basically used to calibrate. A different approach to treat this kind of systems was given

Table 8. Activity and Activity coefficient of Li_2O in the electrolyte at various temperatures

Temperature (K)	$X_{\text{Li}_2\text{O}}$	$a_{\text{Li}_2\text{O}}$	$\gamma_{\text{Li}_2\text{O}}$
1078	0.135	0.077	0.570
1113	0.162	0.092	0.568
1133	0.173	0.102	0.590

and $\gamma_{\text{Li}_2\text{O}}$ is the Pitzer activity coefficient. The activity coefficient values are deduced using the activity values calculated from equation 4 and the composition given in equation 11. These values are listed in Table 8. The activity coefficients calculated from these data agree well with the activity of Li_2O in the electrolyte. They are not too far from unity and follow a regular deviation from ideality. However, the activity values in Pitzer's model of ionic solids exhibit a greater negative deviation from ideality.

The components involved in our system are inorganic molten salts. They are basically ionic in nature. A different approach to treat this kind of systems was given by Temkin [52]. In this method, the activities of ionic compounds can be calculated based on the ion fractions. The relationship for the activity of Li_2O can be expressed as:

$$a_{\text{Li}_2\text{O}} = (x_{\text{Li}^+})^2 \cdot (x_{\text{O}^{2-}}) \cdot \gamma_T \quad (11)$$

where,

$$x_{\text{Li}^+} = \frac{n_{\text{Li}^+}}{n_{\text{Li}^+} + n_{\text{Ca}^{2+}}} = \frac{2n_{\text{Li}_2\text{O}} + n_{\text{LiF}}}{2n_{\text{Li}_2\text{O}} + n_{\text{LiF}} + n_{\text{CaF}_2}} \quad (12)$$

$$x_{\text{O}^{2-}} = \frac{n_{\text{O}^{2-}}}{n_{\text{F}^-} + n_{\text{O}^{2-}}} = \frac{n_{\text{Li}_2\text{O}}}{2n_{\text{CaF}_2} + n_{\text{LiF}} + n_{\text{Li}_2\text{O}}} \quad (13)$$

and γ_T is the Temkin activity coefficient. The activity coefficient values are deduced using the activity values calculated from equation 4 and the expression given in equation 11. These values are listed in Table 9. The activity coefficients calculated from both the approaches indicate that solubility of Li_2O in the electrolyte displays a non-ideal behavior and follows a negative deviation from ideality. However, the approach based on Temkin's model of ionic melts exhibits a smaller negative deviation from ideality.

3.3.3. Activity of Lithium Oxide

The activity levels of Li_2O in the melt were calculated from the data obtained at a number of temperatures and compositions. The activity of Li_2O in the melt was calculated from the data obtained at a number of temperatures and compositions.

Table 9. Temkin activity coefficients of Li_2O in the melt

Temp. (K)	X_{Li^+}	$X_{\text{O}_2^-}$	$X_{\text{Ca}^{2+}}$	X_{F^-}	$(X_{\text{Li}^+})^2 \cdot (X_{\text{O}_2^-})$	$a_{\text{Li}_2\text{O}}$	$\gamma_{\text{T,Li}_2\text{O}}$
1078	0.851	0.115	0.149	0.885	0.083	0.077	0.925
1113	0.859	0.139	0.141	0.861	0.103	0.092	0.897
1133	0.863	0.149	0.137	0.851	0.111	0.102	0.919

3.3.4. Activity of Li_2O in the Melt

In the present case of Li_2O in the melt, the activity of Li_2O in the melt was calculated from the data obtained at a number of temperatures and compositions. The activity of Li_2O in the melt was calculated from the data obtained at a number of temperatures and compositions.

3.3.3. Solubility of Lithium Carbonate

The solubility levels of Li_2CO_3 in the electrolyte was measured by EMF method as a function of temperature in the range of 1063 K to 1093 K. The variation of EMF with the wt % Li_2CO_3 added to the electrolyte at the three experimental temperatures is shown in Figures 10, 11 and 12. The constant EMF observed in the graphs represents the saturation level and gives the maximum solubility of the compound. As explained in the previous section, the solubility levels determined by EMF technique matches very well with the other methods such as chemical analysis. The solubility levels of Li_2CO_3 in LiF-CaF_2 melts at different temperatures are given in Table 10. It increased from 2.95 wt % at 1063 K to 7.57 wt % at 1093 K. The variation of the mole fraction of Li_2CO_3 dissolved in the electrolyte and the temperature is plotted in Figure 13. The linear relationship equation representing the straight line is given by the following equation:

$$\ln X_{\text{Li}_2\text{CO}_3} = 33.43 - \frac{40074.1}{T} \quad (14)$$

3.3.4. Activity of Li_2CO_3 in the Melt

In the previous case of Li_2O , the liquidus temperature of the system $\text{LiF-CaF}_2+\text{Li}_2\text{O}$ (saturated) was 1004 K and the melting point of Li_2O is 2000 K. Therefore, when Li_2O is dissolved below its melting point and above the liquidus temperature of the electrolyte, the existence of the equilibrium between the solid Li_2O and the liquid electrolyte is possible.

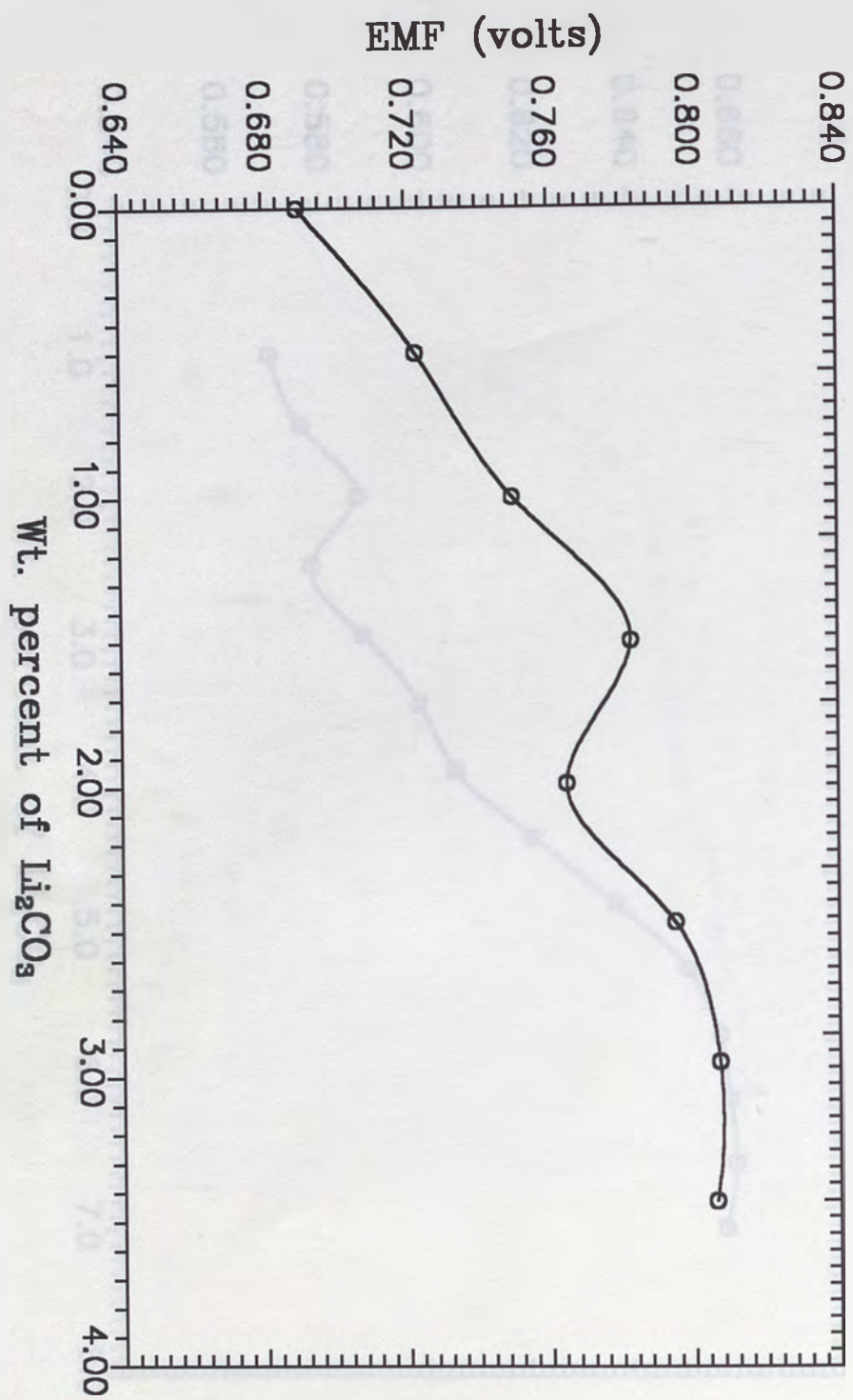


Figure 10. EMF Vs. Wt. percent of Li_2CO_3 dissolved at 1063 K

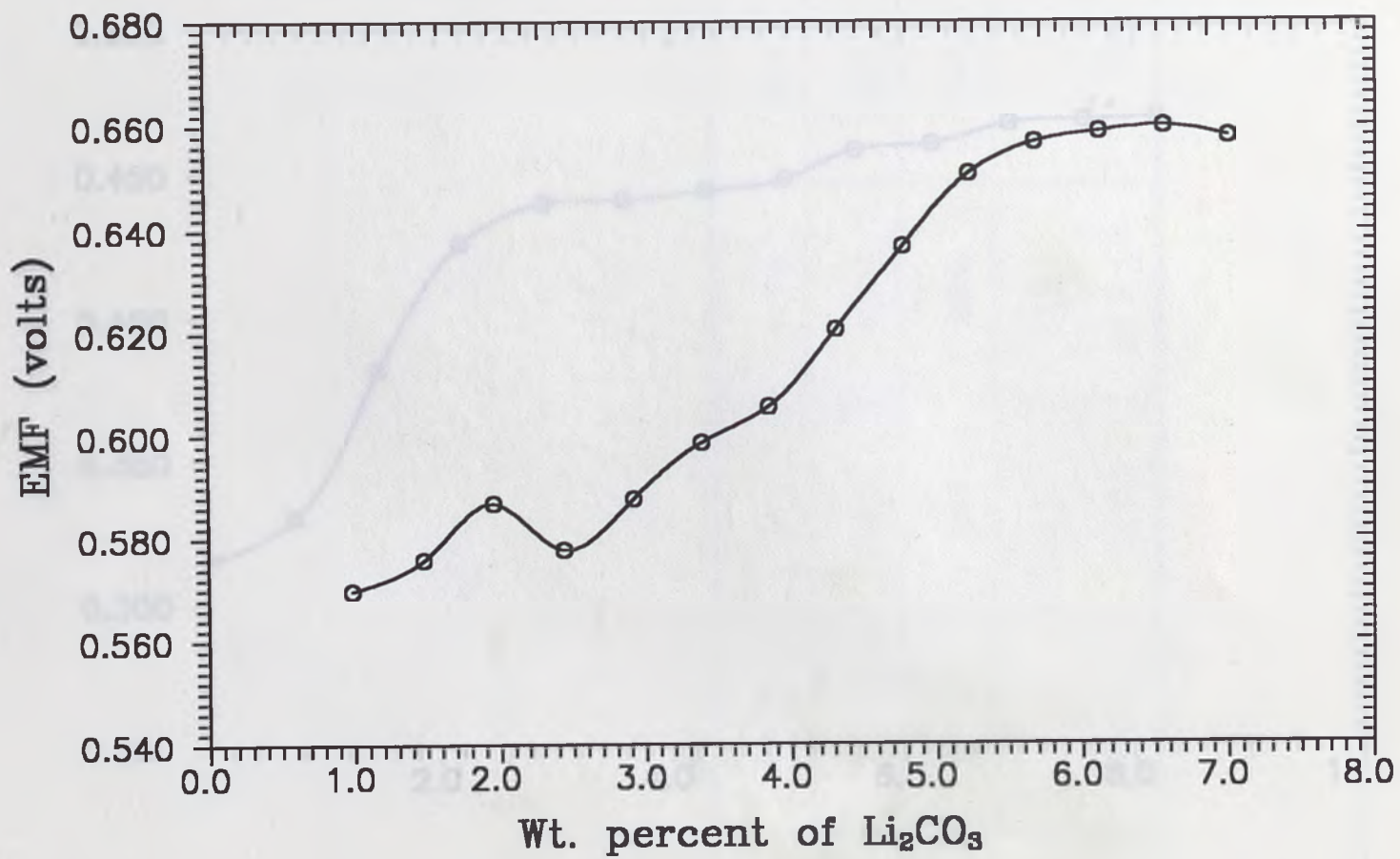


Figure 11. EMF Vs. Wt. percent of Li_2CO_3 dissolved at 1083 K

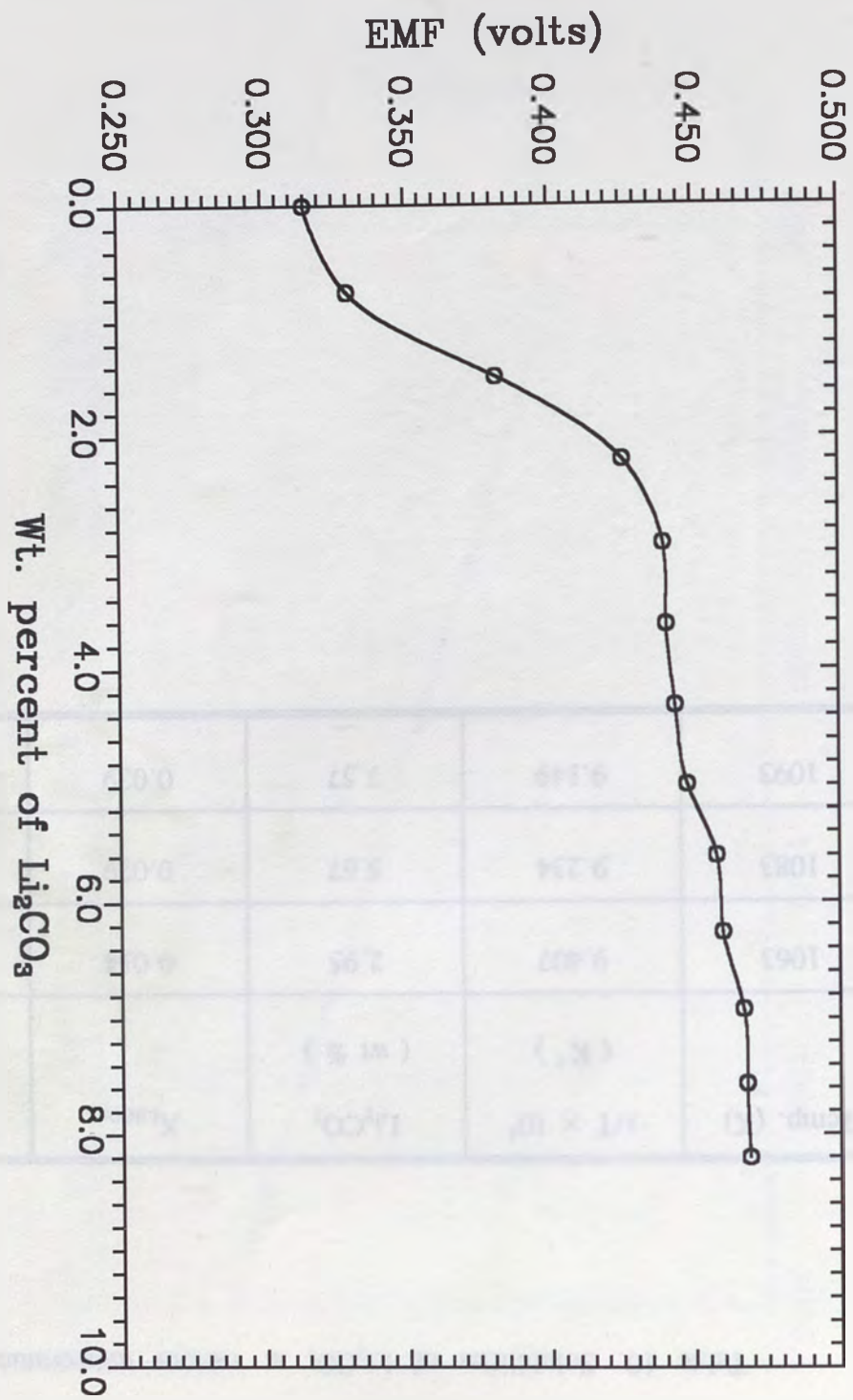


Figure 12. EMF Vs. Wt. percent of Li_2CO_3 dissolved at 1093 K

Table 10. Solubilities of Li_2CO_3 at various temperatures

Temp. (K)	$1/T \times 10^4$ (K^{-1})	Li_2CO_3 (wt %)	$X_{\text{Li}_2\text{CO}_3}$	$\ln X_{\text{Li}_2\text{CO}_3}$
1063	9.407	2.95	0.014	-4.269
1083	9.234	5.67	0.029	-3.541
1093	9.149	7.57	0.039	-3.244

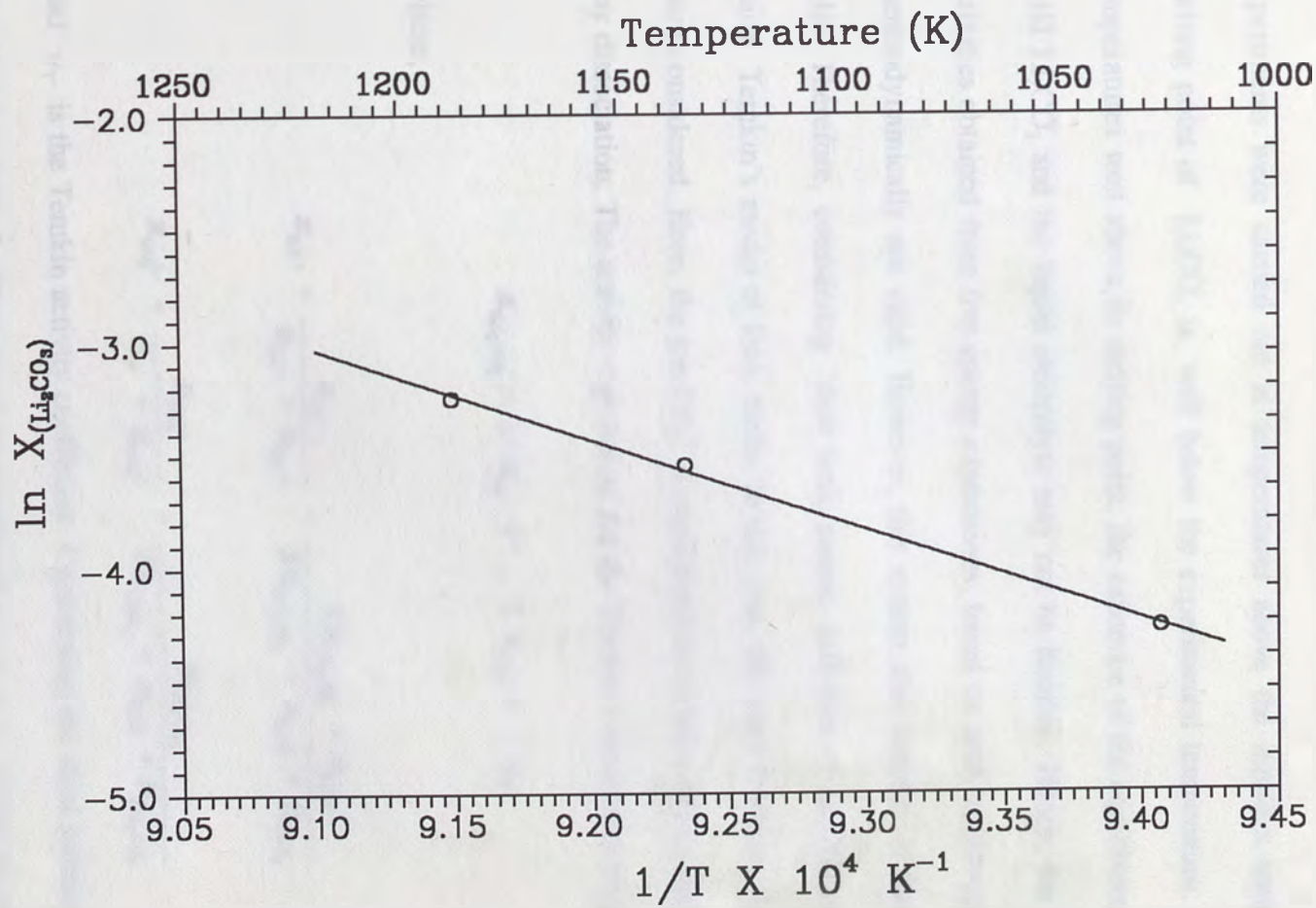


Figure 13. Variation of $\ln X_{Li_2CO_3}$ with temperature

In the case of Li_2CO_3 , the liquidus temperature of the system $\text{LiF-CaF}_2+\text{Li}_2\text{CO}_3$ (saturated) is 1037 K and the melting point of Li_2CO_3 is 993 K. Though, the experiments were carried out at temperatures above the liquidus temperatures, the melting point of Li_2CO_3 is well below the experimental temperature. Therefore, at temperatures well above its melting point, the existence of the equilibrium between the solid Li_2CO_3 and the liquid electrolyte may not be feasible. Hence, the calculation of activities obtained from free energy expressions, based on such equilibrium condition is thermodynamically not valid. However, this system also consists of inorganic molten salts. Therefore, considering their ionic nature, activities of Li_2CO_3 can be deduced using Temkin's model of ionic melts. In this case, the ionic fractions Li^+ and CO_3^{2-} were considered. Here, the ion CO_3^{2-} is considered to be behaving as single ion without any dissociation. The activity expression, for the Temkin's model can be given as below:

$$a_{\text{Li}_2\text{CO}_3} = (x_{\text{Li}^+})^2 \cdot (x_{\text{CO}_3^{2-}}) \cdot \gamma_T \quad (15)$$

where,

$$x_{\text{Li}^+} = \frac{n_{\text{Li}^+}}{n_{\text{Li}^+} + n_{\text{Ca}^{++}}} = \frac{2n_{\text{Li}_2\text{CO}_3} + n_{\text{LiF}}}{2n_{\text{Li}_2\text{CO}_3} + n_{\text{LiF}} + n_{\text{CaF}_2}} \quad (16)$$

$$x_{\text{CO}_3^{2-}} = \frac{n_{\text{CO}_3^{2-}}}{n_{\text{F}^-} + n_{\text{CO}_3^{2-}}} = \frac{n_{\text{Li}_2\text{CO}_3}}{2n_{\text{CaF}_2} + n_{\text{LiF}} + n_{\text{Li}_2\text{CO}_3}} \quad (17)$$

and γ_T is the Temkin activity coefficient. Considering the ideal solution behavior, the Temkin's activity coefficient can be considered as $\gamma_T = 1$. Using the expression (15), the activity values were calculated for $\gamma_T = 1$. The deduced activity values are given

in Table 11. The calculated activity values indicates that, the dissolution of Li_2CO_3 in the electrolyte displays a non-ideal behavior. The Temkin's ideal solution behavior approach shows a negative deviation from the ideal behavior by the conventional approach.

A comparison of the solubility data of different oxides in the fluoride melts studied by various investigators is shown in Figure 14. However, the different components involved in the electrolytes in these systems and variation in the molar ratios of the compounds dissolved restricts a strict comparison to be made among these systems. Nevertheless, some general observations can be made by comparing these data. The solubility of Li_2O in fluoride melts is very much higher than any other compounds. The solubility levels of Li_2CO_3 is very much closer to many of these compounds.

3.3.5. Liquidus Temperatures

The liquidus temperatures were determined by the cooling curve method as described in section 3.2.4. The liquidus temperature of the eutectic mixture of the electrolyte LiF-CaF_2 was determined to be 1047 K which is very close to the established value of 1042 K. The liquidus temperature of the electrolyte saturated with Li_2CO_3 was determined to be 1037 K. The cooling curve for the $\text{LiF-CaF}_2\text{-Li}_2\text{CO}_3$ (sat.) is shown in Figures 15. The various liquidus temperatures are given in Table 12.

Table 11. Temkin activities of Li_2CO_3 in the electrolyte

Temp. (K)	X_{Li^+}	$X_{\text{Ca}^{2+}}$	$X_{\text{CO}_3^{2-}}$	X_{F^-}	$a_{\text{T},\text{Li}_2\text{CO}_3}$
1063	0.810	0.190	0.012	0.988	7.873×10^{-3}
1083	0.816	0.184	0.024	0.976	15.980×10^{-3}
1093	0.819	0.181	0.032	0.968	21.464×10^{-3}

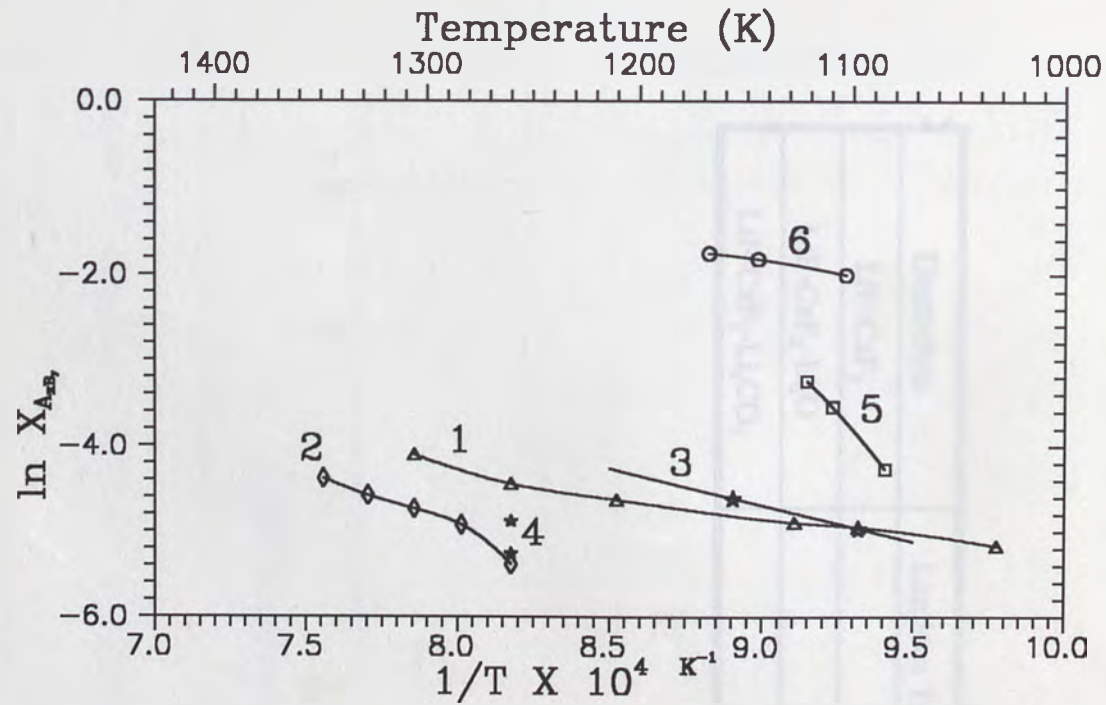
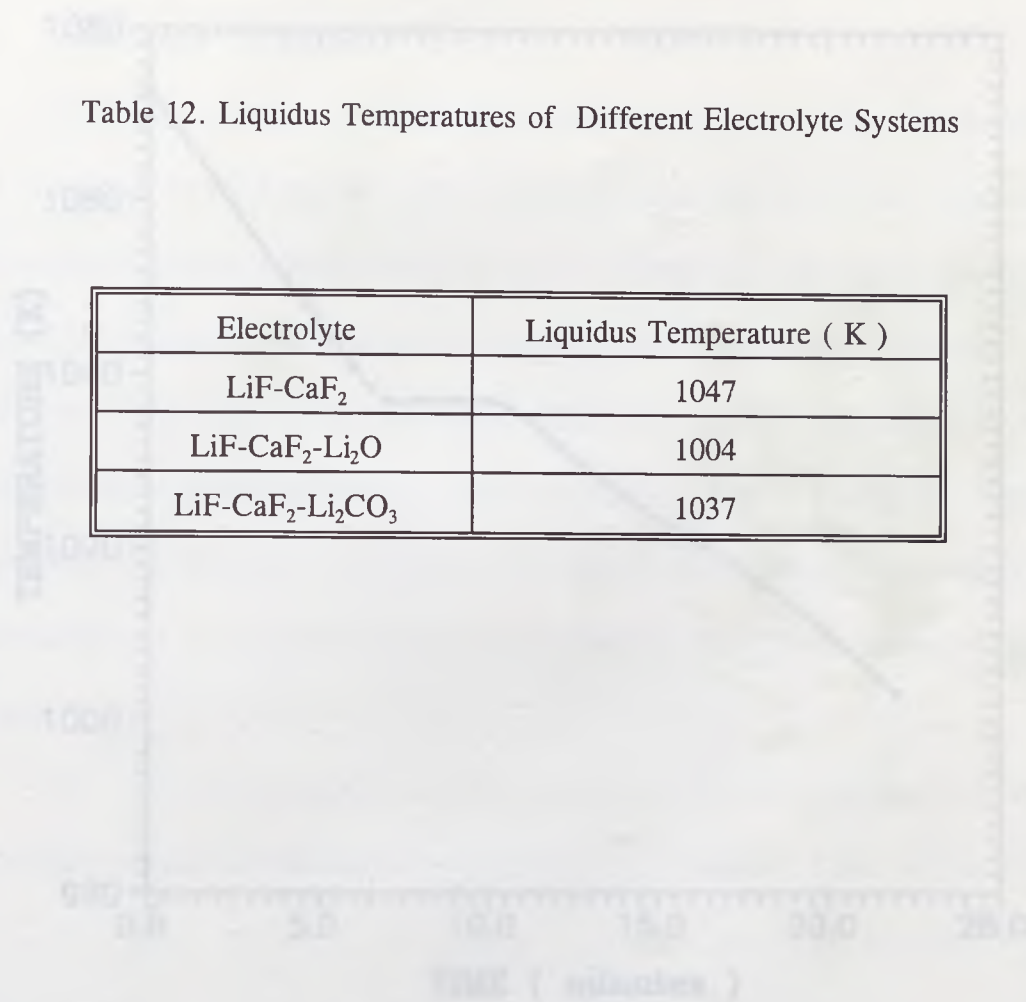


Figure 14. Solubilities of Different Oxides in Fluoride Melts

- | | | | |
|-----|--------------------------------------|-----|--|
| (1) | Y_2O_3 in $LiF-YF_3$ | (4) | La_2O_3 in LaF_3-BaF_2-LiF |
| (2) | SnO_2 in $NaF-AlF_3-CaF_2-Al_2O_3$ | (5) | Li_2CO_3 in $LiF-CaF_2$ (Present Work) |
| (3) | CeO_2 in CeF_3-BaF_2-LiF | (6) | Li_2O in $LiF-CaF_2$ (Present Work) |

Table 12. Liquidus Temperatures of Different Electrolyte Systems

Electrolyte	Liquidus Temperature (K)
LiF-CaF ₂	1047
LiF-CaF ₂ -Li ₂ O	1004
LiF-CaF ₂ -Li ₂ CO ₃	1037

Figure 11. Heatflow Temperature of LiF-CaF₂-Li₂CO₃ (wt.%) 100

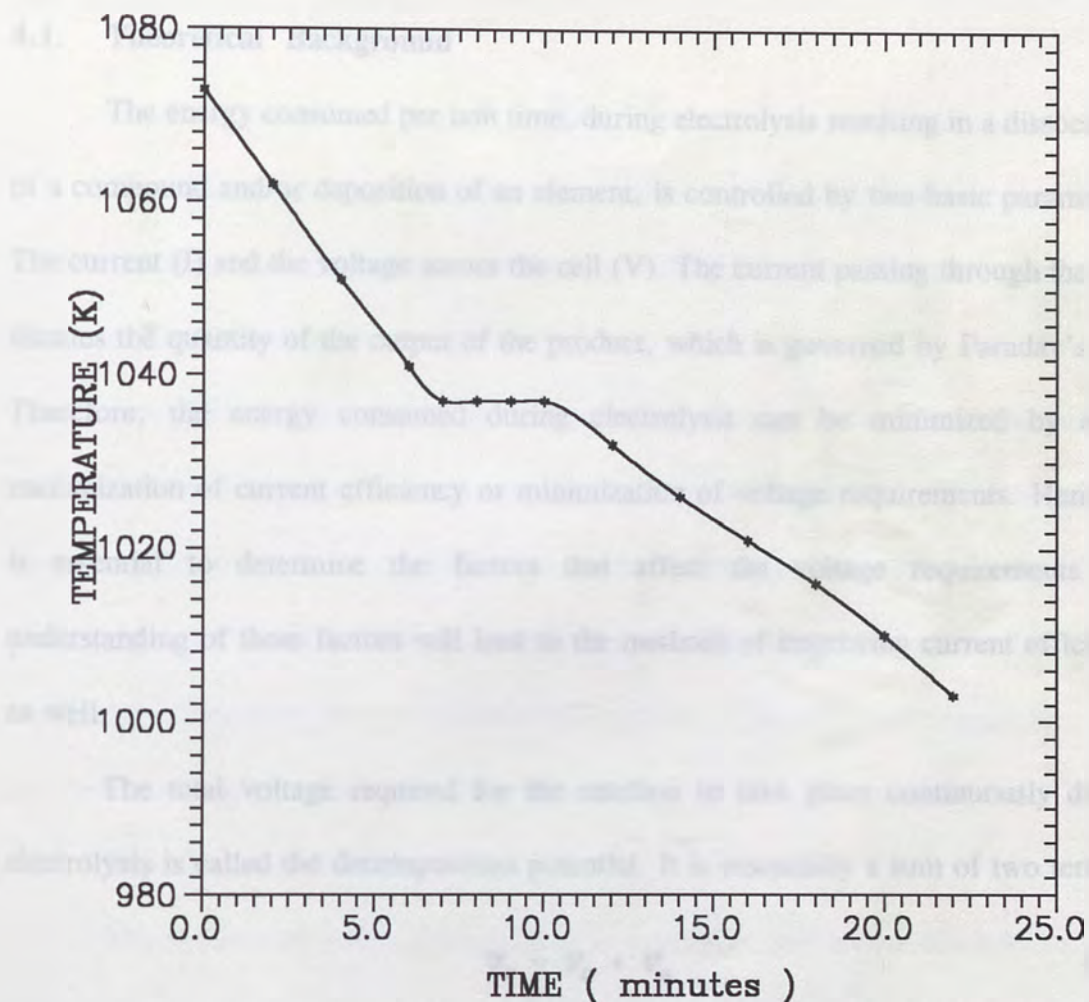


Figure 15. Liquidus Temperature of $\text{LiF-CaF}_2\text{-Li}_2\text{CO}_3$ (sat.) Melt

4.0. ANODIC OVERVOLTAGE MEASUREMENTS DURING THE ELECTROLYSIS OF LITHIUM COMPOUNDS IN THE LiF-CaF₂ MELTS

4.1. Theoretical Background

The energy consumed per unit time, during electrolysis resulting in a dissociation of a compound and/or deposition of an element, is controlled by two basic parameters. The current (I) and the voltage across the cell (V). The current passing through the cell, dictates the quantity of the output of the product, which is governed by Faraday's law. Therefore, the energy consumed during electrolysis can be minimized by either maximization of current efficiency or minimization of voltage requirements. Hence, it is essential to determine the factors that affect the voltage requirements. An understanding of these factors will lead to the methods of improving current efficiency as well.

The total voltage required for the reaction to take place continuously during electrolysis is called the decomposition potential. It is essentially a sum of two terms.

$$V_T = V_D + V_\eta \quad (18)$$

where, V_T is the total voltage required; V_D is the thermodynamic voltage required for the overall cell reaction; and V_η is the overvoltages. Since the thermodynamic voltage requirement is more or less a fixed quantity for a given temperature that can be obtained from the gibbs energy values of the reaction, it is the overvoltage that eventually affects the voltage requirements of the reaction.

When a current flows through an electrode, its potential V_i , assumes a different value from that in the absence of current, V_o . Therefore, in simple terms the overvoltage

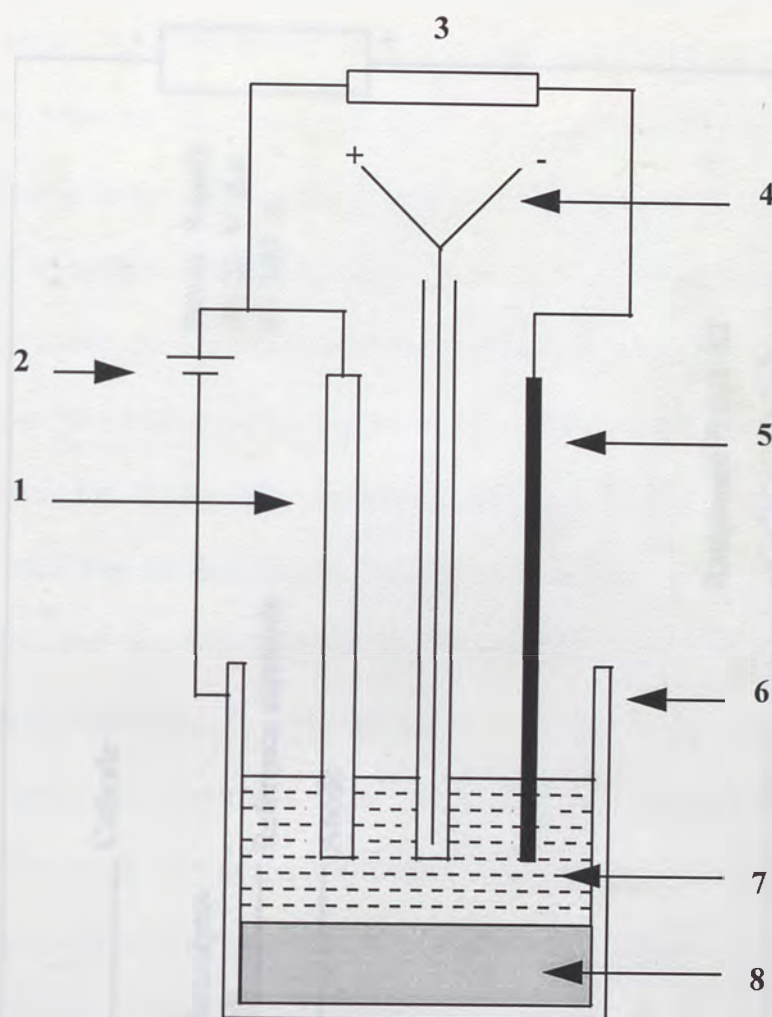
can be defined as the difference between an equilibrium and a non-equilibrium potential and denoted by ' η ' is given as:

$$\eta = V_{(i)} - V_{(e)} \quad (19)$$

The total overvoltage may be expressed as the sum of different contributing factors, such as: (1) activation overvoltage resulting from the slow electron transfer reaction; (2) resistance overvoltage arising from the resistance of the electrolyte; (3) concentration overvoltage due to the concentration changes in the electrolyte near the vicinity of the electrodes. The total overvoltage can be determined experimentally by measuring the potential of the individual electrodes at a given current density. In the present case, the dissolved lithium compound is dissociated at the anode surface during electrolysis. Therefore, the experimental determination of anodic overvoltage is important for understanding the efficiency of the process.

4.2. Experimental Studies

The anode used in the present study is a graphite rod with a diameter of 12.7 mm. The anodic overvoltage on the graphite anode during the electrochemical dissociation of lithium carbonate in LiF-CaF₂ electrolyte was determined. The furnace setup, described in section 3.4 for the solubility studies, was used here. The schematic diagram of the overvoltage measurements setup is shown in Figure 16. The outline of the electrical circuit for the electrochemical cell is shown in Figure 17. The chemicals, calcium fluoride, lithium fluoride and lithium carbonate were obtained from the same source as mentioned earlier.



- | | |
|------------------------|----------------------|
| 1. Anode | 2. Power supply |
| 3. Multimeter | 4. Thermocouple |
| 5. Reference electrode | 6. Graphite crucible |
| 7. Electrolyte | 8. Aluminum |

Figure 16. Schematic diagram of the overvoltage measurement setup

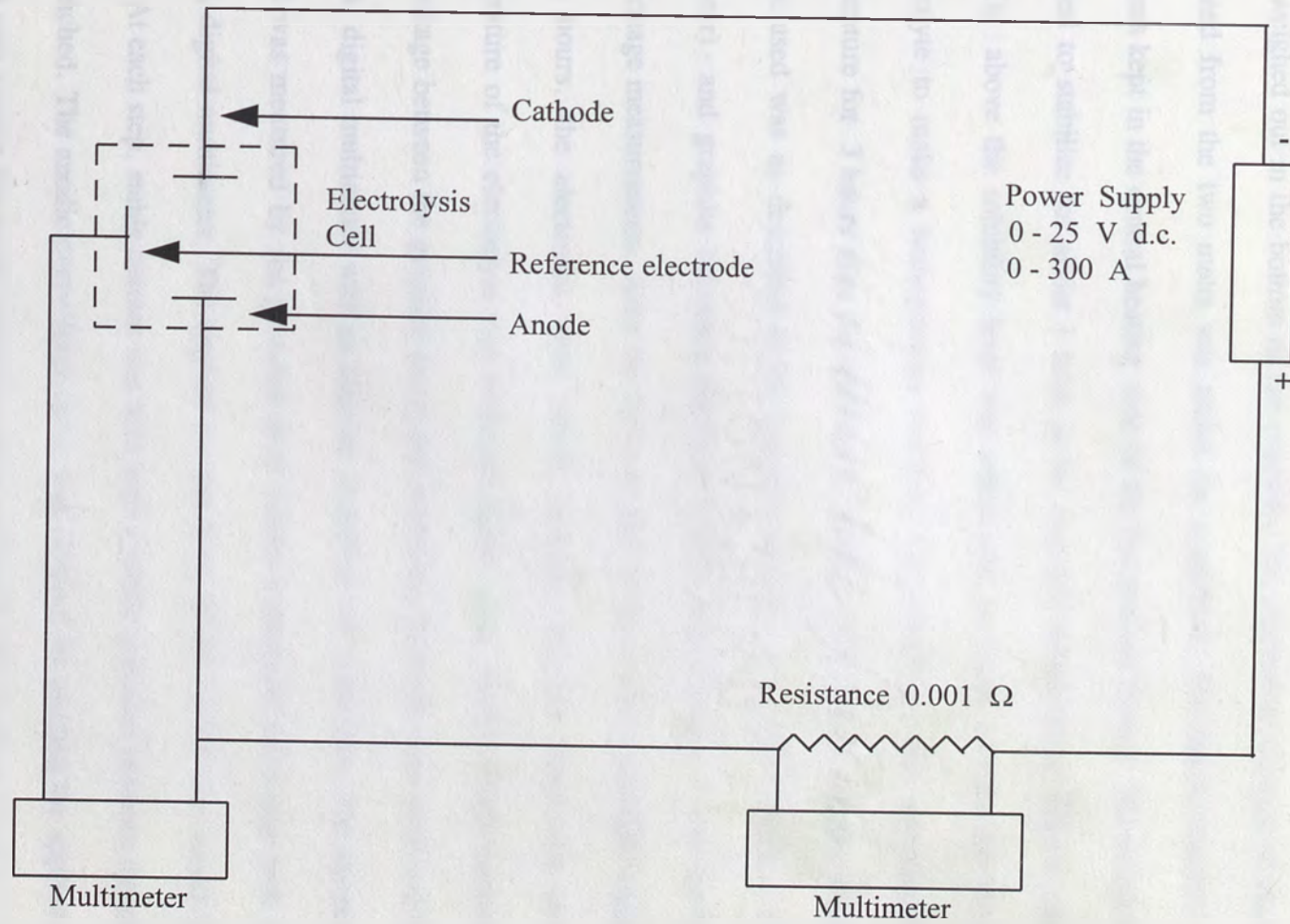


Figure 17. Schematic outline of the electric circuit for overvoltage measurements

The preparation of the electrolyte was done by the same procedure described in section 3.4. Pure aluminum shots of about 150 g, obtained from Aldrich Chemical Co., was weighed out in the bottom of the crucible. The electrolyte mixture of about 400 g obtained from the two melts was added the aluminum. The whole crucible with its contents kept in the central heating zone of the furnace and melted. The entire melt was allowed to stabilize for about 1 hour at the required temperature. Excess quantity of Li_2CO_3 above the solubility level was added and inert gas was purged through the electrolyte to make a homogeneous mixture. The electrolyte was maintained at the temperature for 3 hours after the addition of lithium carbonate. The argon gas cleaning circuit used was as described in the previous section. A graphite anode (12.7 mm diameter) and graphite reference electrode (6.35 mm diameter) was used for the overvoltage measurements. After the melt was kept at the required stabilized temperature for 3 hours, the electrodes were slowly lowered into the electrolyte melt. The temperature of the electrolyte was measured again using Pt-Pt/10%Rh thermocouple. The voltage between the graphite anode and reference electrode was measured by a HP 3466A digital multimeter with an internal resistance of 10 M-ohm. The current in the circuit was measured by the potential drop across a standard resistance with a Fluke 8010A digital multimeter. The applied current level in the circuit was raised in small steps. At each step, stable current was held until a steady potential between the electrode was reached. The anodic overvoltage curve was obtained by plotting the applied current at each step against the steady potential values measured. The applied current was found to be very much steady with a scatter of 0.01 amperes.

4.3. Results and Discussion

4.3.1. Overvoltage of LiF-CaF₂ + Li₂CO₃ System

The experimental measurement of anodic overvoltage on the graphite electrode was carried out. The system studied is the same as that of solubility studies. The electrolyte LiF-CaF₂ was saturated with Li₂CO₃. The overvoltage measured at various current level for Li₂CO₃ saturated system is shown in Table 12. The current densities calculated from the applied current levels, are also tabulated. At different temperatures studied, the variation of overvoltage η with log current density showed a linear relationship upto a limiting current density level. This kind of linear variation of overvoltage with log current density is described as Tafel behavior. The plot between overvoltage at log current density from experimental data at 1093 K, is shown in Figure 18.

The variation of η Vs $\log i$ was found to be linear upto a current density value of 0.01 A/cm² and above this level it is non-linear upto 0.05 A/cm². When the current level was increased beyond this range, sudden changes were observed, with a large change in the voltage level for a small change in current density. Further increase in the current level in the circuit, resulted in the localized heating and cathode became red hot making the measurements difficult.

Table 13. Anodic overvoltage measurements for Li_2O system at 1093 K

Current (I) (Amperes)	Potential (V) (Volts)	Current density (i) (A / cm ²)	log i
0.003	0.095	2.669×10^{-4}	-3.574
0.012	0.180	1.068×10^{-3}	-2.972
0.027	0.405	2.402×10^{-3}	-2.619
0.044	0.805	3.914×10^{-3}	-2.407
0.064	1.120	5.693×10^{-3}	-2.245
0.086	1.320	7.651×10^{-3}	-2.116
0.098	1.405	8.712×10^{-3}	-2.060
0.108	1.515	9.608×10^{-3}	-2.017
0.119	1.620	0.011	-1.975
0.132	2.098	0.012	-1.930
0.144	2.290	0.013	-1.892
0.164	2.350	0.015	-1.836
0.185	2.920	0.017	-1.784
0.207	3.275	0.018	-1.735
0.255	4.054	0.023	-1.644
0.310	4.840	0.028	-1.559
0.515	8.160	0.046	-1.339
0.750	11.010	0.067	-1.176

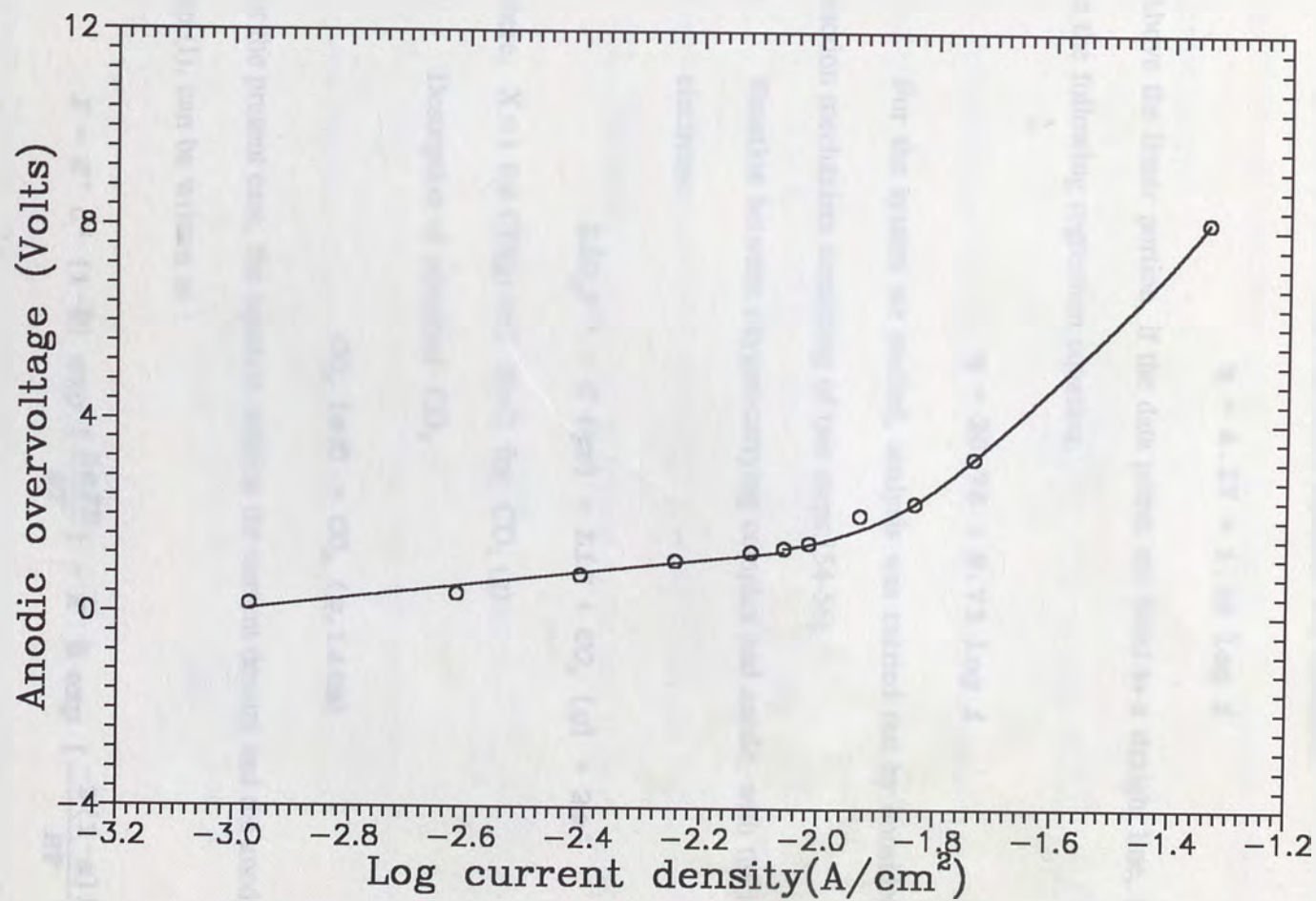


Figure 18. Variation of Overvoltage Vs Log current density on graphite anode during electrolysis of $\text{LiF-CaF}_2 + \text{Li}_2\text{CO}_3$ (sat.) melt at 1093 K.

From the Figure 18, between η Vs $\log i$ at 1093 K, for the linear portion called Tafel region, the following regression equation was obtained.

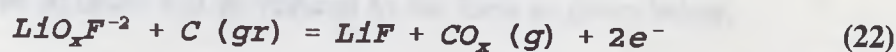
$$\eta = 4.17 + 1.38 \log i \quad (20)$$

Above the linear portion, if the data points are fitted to a straight line, then it resulted in the following regression equation.

$$\eta = 20.76 + 9.73 \log i \quad (21)$$

For the system we studied, analysis was carried out by considering the anode reaction mechanism consisting of two steps:[54-56]

- I. Reaction between oxygen-carrying complex and anode, with the transfer of two electrons:



where, $X=1$ for $CO(g)$ and $X=2$ for $CO_2(g)$.

- II. Desorption of adsorbed CO_x :



For the present case, the equation relating the current density and the anode potential for step (I), can be written as :

$$I = K^+ C^2 (1-\theta) \exp \left[\frac{2\alpha FE}{RT} \right] - K^- \theta \exp \left[\frac{-2(1-\alpha) FE}{RT} \right] \quad (24)$$

where, C is the concentration of the oxygen carrying complex, LiO_xF^{-2} , K^+ and K^- are the rate constants for the anodic and cathodic reactions respectively, θ is the surface

coverage of CO_x (ad), E is the anode potential, α is the the transfer coefficient, R is the gas constant, T is the absolute temperature and F is the faraday's constant. At equilibrium potential the exchange current density for the present case can be written as below:

$$i_o = K^+ C^2 (1-\theta_o) \exp \left[\frac{-2\alpha F E_e}{RT} \right] = K^- \theta_o \exp \left[\frac{-2(1-\alpha) F E_e}{RT} \right] \quad (25)$$

By definition, the overvoltage is $\eta = E - E_e$, which is same as that of equation 19.

Therefore, dividing equation 24 by 25, the expression obtained is:

$$I = i_o \left\{ \left[\frac{1-\theta}{1-\theta_o} \right] \exp \left[\frac{2\alpha F \eta}{RT} \right] - \frac{\theta}{\theta_o} \exp \left[\frac{-2(1-\alpha) F \eta}{RT} \right] \right\} \quad (26)$$

Assuming that no accumulation of CO_x products occurs, the surface coverage becomes $\theta = \theta_o$. The above equation will be reduced to the form as given below.

$$I = i_o \left\{ \left[\exp \left[\frac{2\alpha F \eta}{RT} \right] - \exp \left[\frac{-2(1-\alpha) F \eta}{RT} \right] \right] \right\} \quad (27)$$

For the higher anodic current densities, only the second term is significant and the equation simplifies to the following forms:

$$\eta = - \frac{2.303RT}{2\alpha F} \log i_o + \frac{2.303RT}{2\alpha F} \log I \quad (28)$$

$$\eta = a + b \text{Log } I \quad (29)$$

Equation 28 is the Tafel equation, for a charge transfer controlled two electron reaction.

The plot between η Vs $\log i$ gives the Tafel constants a and b . The slope is $b =$

($2.303 RT / 2\alpha F$) and the intercept on the ordinate gives the other constant $a = (- 2.303 RT / 2\alpha F) \log i_0$. From the experimental data, the plot was made as shown in Figure 18 and the equation corresponding to the Tafel region is given by the equation 20. Comparing the equations 20 and 29, the Tafel constants were deduced as $a = 4.17$ and $b = 1.38$. From this experimentally derived values of a and b , the exchange current density and charge transfer coefficient were determined.

Above the Tafel region, the plot of η Vs $\log i$ follows a non-linear relationship at higher current densities. This might be due to slow removal of adsorbed CO_x products from the anode surface as given by Step II. A Langmuir adsorption behavior of CO_x products on to the surface of the graphite anode is assumed. The current density expression for the reaction in Step II, following this behavior can be given as:

$$i = K_d \theta - K_a P_{CO_x} (1-\theta) \quad (30)$$

where, K_d and K_a are rate constants for the desorption and adsorption reactions of CO_x respectively. θ is the surface coverage and P_{CO_x} partial pressure of CO_x gases. At equilibrium conditions, a limiting current phenomenon will occur when $\theta = 1$. i.e., when the surface is fully covered. Considering the exchange current density phenomenon at equilibrium, the expressions for adsorption and desorption for the equation 30, can be written as below:

$$i_r = K_d \theta_o \quad (31)$$

$$i_r = K_a P_{CO_x} (1 - \theta_o) \quad (32)$$

Substituting the values of K_d and K_a from the equation 31 and 32 into the expression 30 and rearranging the terms, we get:

$$i = i_r \left[\frac{\theta}{\theta_o} - \frac{(1-\theta)}{(1-\theta_o)} \right] \quad (33)$$

From this expression, the value of θ can be obtained as given below.

$$\theta = \frac{i}{i_r} \theta_o (1 - \theta_o) + \theta_o \quad (34)$$

It has been established that, for many electrochemical systems the transfer coefficients for the anodic and cathodic reactions are same and equal to 0.5. Therefore, assuming that, $\alpha = 1/2$, the exchange current density equation 26 derived earlier will be reduced to the following:

$$i = i_o \left(\frac{1-\theta}{1-\theta_o} \right) \exp \left(\frac{F\eta}{RT} \right) - \frac{\theta}{\theta_o} \exp \left(\frac{-F\eta}{RT} \right) \quad (35)$$

Substituting the value of θ from equation 34 into the above expression and considering only the anodic term at higher anodic current densities where the cathodic term insignificant, equation 35 reduces to the following:

$$\frac{1}{i} = \frac{1}{i_o} \exp \left(\frac{-F\eta}{RT} \right) + \frac{\theta_o}{i_r} \quad (36)$$

The exchange current density i_0 , for the reaction of step I was deduced using the plot between $1/i$ Vs $\exp(-F\eta / RT)$. The linear equation obtained from this plot will have the similar form of equation 36. Therefore, the intercept value in the linear equation corresponds to the constant term θ_0 / i_r . If the value of θ_0 / i_r is substituted into the expression for θ in the equation 33, the limiting current density i_L can be evaluated by setting $\theta = 1$, where limiting current phenomenon occurs due to complete surface coverage.

From the experimental data of the Tafel region, the exponential term in equation 36, $\exp(-\eta F/RT)$ was calculated at each overvoltage values. These values are given in Table 13, along with the corresponding $1/i$ values. The plot between $1/i$ and the term $\exp(-\eta F/RT)$ is shown in Figure 19. From this plot, the following straight line equation is obtained.

$$\frac{1}{i} = 4.86 \times 10^4 \exp\left(\frac{-\eta F}{RT}\right) + 93.65 \quad (37)$$

The values of $1/i$ and $\exp(-\eta F/RT)$ were calculated in the current density range between 0.008 A/cm^2 to 0.012 A/cm^2 . Comparing the equation 37 with equation 36 the values of θ_0/i_r and i_0 are deduced as, $(\theta_0/i_r) = 4.86 \times 10^4$ and $i_0 = 93.65 \text{ A/cm}^2$. At equilibrium, it can be assumed that $\theta = 1$. For this condition, as explained earlier, substituting the value of θ_0/i_r in the equation 34, it can be deduced that:

$$93.65 i_L = 1$$

and

$$i_L = 0.011 \text{ A/cm}^2$$

Table 14. Calculated values of $1/i$ and $\text{Exp}(-F\eta/RT)$ of Li_2O system for the limiting current density determination

Overvoltage, η (Volts)	Current density, i (A / cm^2)	$1 / i$	$\text{Exp}(-F\eta / RT)$
1.320	7.6506×10^{-3}	130.71	8.171×10^{-7}
1.405	8.7181×10^{-3}	114.70	3.313×10^{-7}
1.515	9.6077×10^{-3}	104.08	1.030×10^{-7}
1.620	0.0106	94.34	3.378×10^{-8}
2.098	0.0117	85.47	2.110×10^{-10}

Figure 15. Variation of the factor $\text{Exp}(-F\eta/RT)$ with current density at 295 K for Li_2O saturated system.

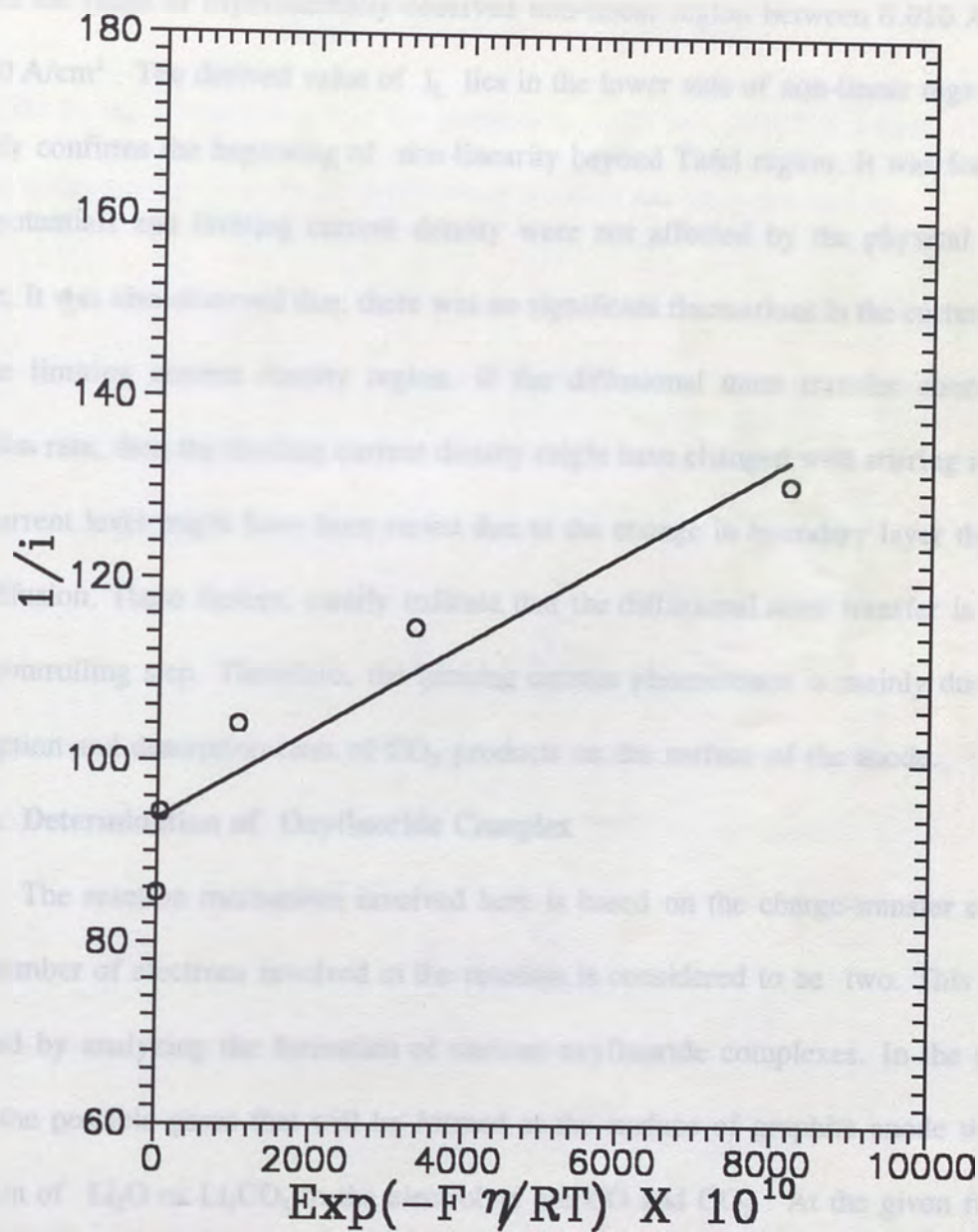


Figure 19. Variation of the factor $\text{Exp}(-F\eta/RT)$ with current density at 1093 K for Li_2CO_3 saturated system

The derived value of limiting current density above, i.e., 0.011 A/cm^2 , falls within the range of experimentally observed non-linear region between 0.010 A/cm^2 to 0.050 A/cm^2 . The derived value of i_L lies in the lower side of non-linear region. This clearly confirms the beginning of non-linearity beyond Tafel region. It was found that overpotentials and limiting current density were not affected by the physical stirring effect. It was also observed that, there was no significant fluctuations in the current levels in the limiting current density region. If the diffusional mass transfer controls the reaction rate, then the limiting current density might have changed with stirring and also the current level might have been varied due to the change in boundary layer thickness by diffusion. These factors, clearly indicate that the diffusional mass transfer is not the rate controlling step. Therefore, the limiting current phenomenon is mainly due to the adsorption and desorption rates of CO_x products on the surface of the anode.

4.3.2. Determination of Oxyfluoride Complex

The reaction mechanism involved here is based on the charge-transfer control. The number of electrons involved in the reaction is considered to be two. This can be verified by analyzing the formation of various oxyfluoride complexes. In the present case, the possible gases that will be formed at the surface of graphite anode with the addition of Li_2O or Li_2CO_3 to the electrolyte are CO and CO_2 . At the given reaction temperature, 1093 K , the composition of the gaseous products can be calculated from the Gibbs energy values as shown below.

Considering the reaction at the graphite electrode:



At 1093 K, the Gibbs energy for the reaction is , $\Delta G^\circ = - 19197.9 \text{ J/mole}$ [52]. This Gibbs energy value in terms of equilibrium constant can be expressed as:

$$\Delta G^\circ = - RT \ln K \quad (39)$$

Substituting the values of ΔG° , R and T , the value of the equilibrium constant is calculated as, $K = 8.27$. The equilibrium constant in terms of reactants and products for the reaction in equation 38, can be written as:

$$K = \frac{P_{CO}^2}{P_{CO_2} a_C} \quad (40)$$

Considering the activity of solid graphite electrode as $a_C = 1$, the equilibrium constant becomes:

$$K = \frac{P_{CO}^2}{P_{CO_2}} \quad (41)$$

The total pressure is considered as equal to 1 bar.

$$P_{CO} + P_{CO_2} = P_T = 1 \quad \text{bar} \quad (42)$$

Substituting the value of the equilibrium constant K and the value of P_{CO_2} from the above equation into the expression for K , the following equation is obtained.

$$P_{CO}^2 + 8.27 P_{CO} - 8.27 = 0 \quad (43)$$

Solving this equation, the values of P_{CO} and P_{CO_2} are deduced as $P_{CO} = 0.9 \text{ atm}$ and

$P_{\text{CO}_2} = 0.1$ atm. These calculations indicate that both CO and CO₂ gases are evolved during the reaction in the melt at that temperature. However, the amount of CO₂ produced is very small when compared to CO.

The general reaction given in equation 33, for the first stage of the reaction mechanism can now be written for the CO and CO₂ gas evolution as below.

For $x = 1$,



and for $x = 2$,



A detailed analysis was made on the various possible oxyfluoride complexes that can react to form CO and CO₂ gases. The above mentioned oxyfluoride complexes are the only two forms that can react with carbon to give out stable compounds. The reactions involving both these complexes to give out CO and CO₂ gases are characterized by a two electron transfer. The above analysis indicates that the electrolyte melt is basically consisting of LiO_xF²⁻ oxyfluoride complex. Therefore, it can be concluded that the electrolyte LiF-CaF₂ + Li₂CO₃ at 1093 K, consists of 90 % of LiOF²⁻ and 10 % of LiO₂F²⁻ complexes.

4.3.3. Overvoltage of LiF-CaF₂ + Li₂O System

The experimental measurements of anodic overvoltages in the LiF-CaF₂ + Li₂O system was carried in a similar way to that of LiF-CaF₂ + Li₂CO₃ system at 1093 K. The overvoltages and current densities measured at different current levels are shown in Table 14. The variation of overvoltage η , with log current density i , showed a linear relationship upto a limiting current density level. The plot between η Vs log i of the experimental data of Table 14, is shown in Figure 20. A linear dependence was observed upto 0.50 A/cm² and limiting current phenomenon was observed between 0.50 A/cm² and 0.71 A/cm². Beyond this region the line deviated from straight line. At higher current densities abrupt changes were observed with a small change in current density. From the Tafel region, the following regression equation was obtained[57].

$$\eta = 1.32 + 0.84 \log i \quad (46)$$

An analysis can be carried out, considering the reaction mechanism consisting of two steps similar to as explained earlier for the LiF-CaF₂ + Li₂CO₃ system. The first step is the reaction between the oxygen carrying complex and the anode and the second step is the desorption of absorbed CO_x products.

At higher current densities, beyond Tafel limit, a Langmuir adsorption of CO_x products is assumed. The limiting current density, i_L can be obtained from the equations 33 and 36, similar to the procedure adopted for LiF-CaF₂ + Li₂CO₃ system. From the experimental data of Tafel region, the values of the terms $\exp(-\eta F/RT)$ and $1/i$ were calculated and given in Table 15.

Table 15. Anodic overvoltage measurements for Li_2CO_3 system at 1093 K

Current (I) (Amperes)	Potential (V) (Volts)	Current density (i) (A / cm ²)	log i
1.03	0.42	0.088	-1.050
1.62	0.60	0.138	-0.859
2.62	0.83	0.223	-0.650
3.42	0.84	0.292	-0.535
4.43	0.95	0.378	-0.422
5.49	1.04	0.468	-0.329
8.43	1.32	0.719	-0.143
9.15	1.48	0.781	0.108
12.86	1.67	1.097	0.040
13.95	1.88	1.190	0.076

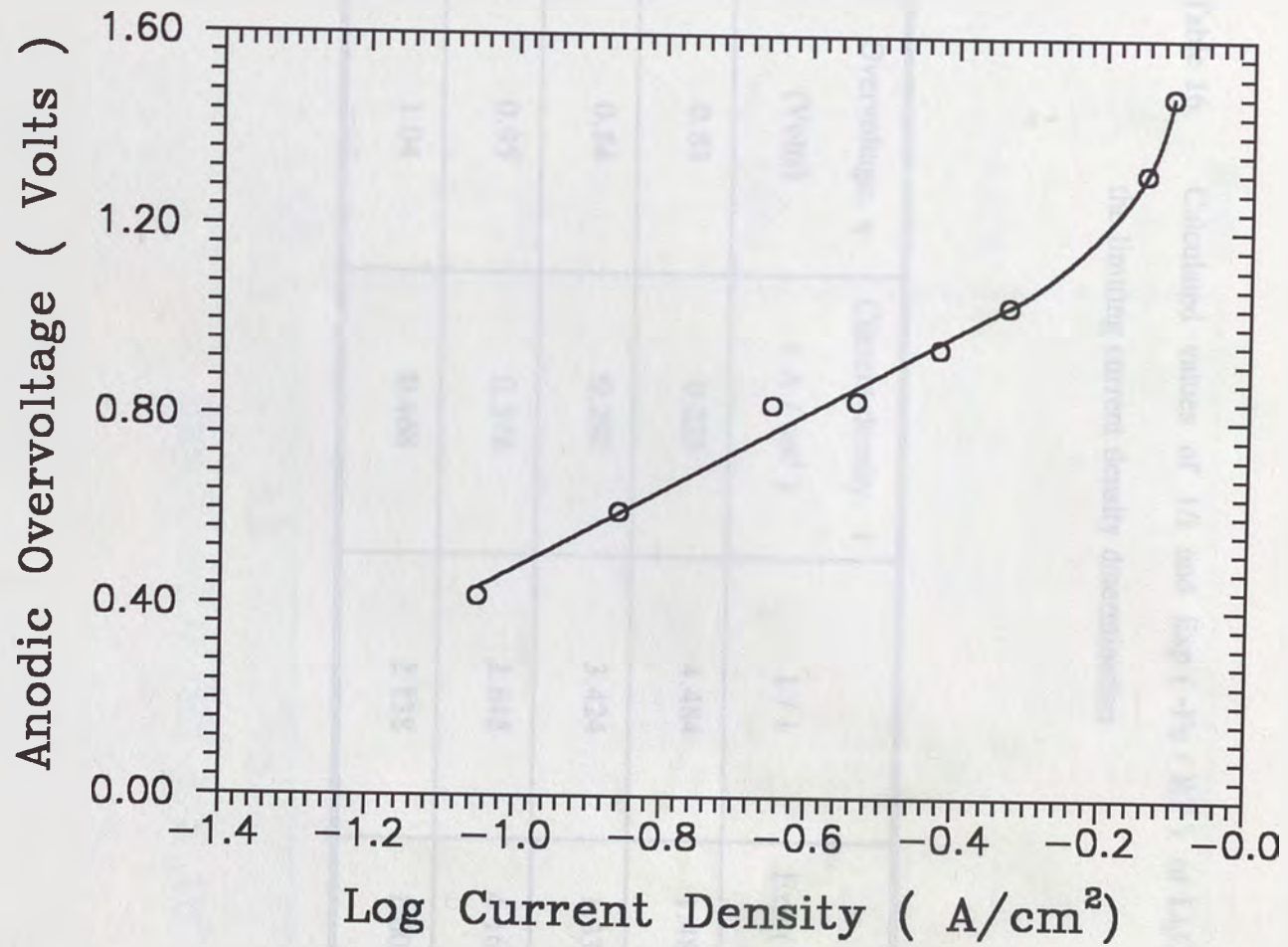


Figure 20. Variation of Overvoltage Vs Log current density on graphite anode during electrolysis of $\text{LiF-CaF}_2 + \text{Li}_2\text{CO}_3$ (sat.) melt at 1093 K.

Table 16. Calculated values of $1/i$ and $\text{Exp}(-F\eta/RT)$ of Li_2CO_3 system for the limiting current density determination

Overvoltage, η (Volts)	Current density, i (A / cm ²)	$1 / i$	$\text{Exp}(-F\eta / RT)$
0.83	0.223	4.484	1.488×10^{-4}
0.84	0.292	3.424	1.338×10^{-4}
0.95	0.378	2.645	4.162×10^{-5}
1.04	0.468	2.138	1.600×10^{-5}

Figure 11. Variation of the factor $\text{Exp}(-F\eta/RT)$ with current density at 298 K for Li_2CO_3 saturated system

The plot between $1/i$ and $\exp(-F\eta/RT)$ as shown in Figure 21, gives the following straight line equation.

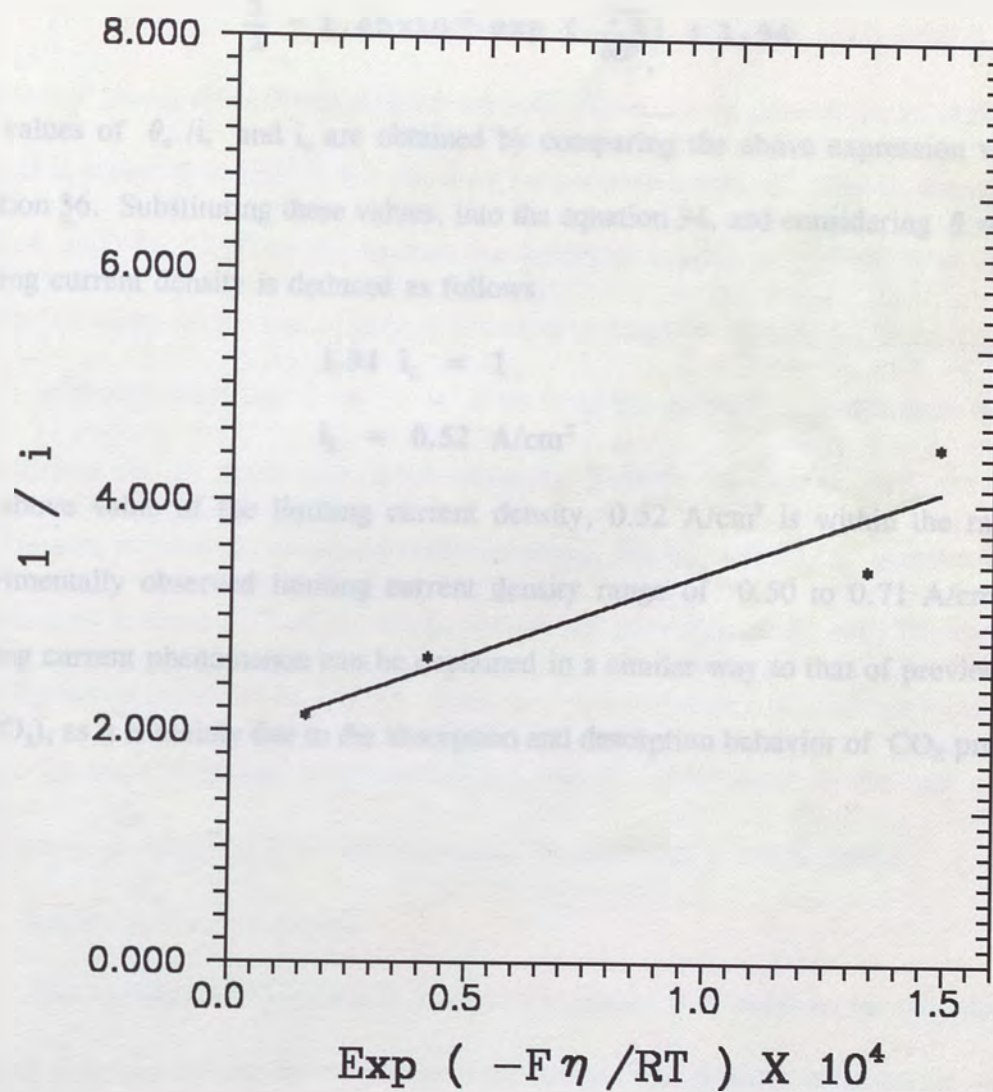


Figure 21. Variation of the factor $\text{Exp}(-F\eta/RT)$ with current density at 1093 K for Li_2O saturated system

The plot between $1/i$ and $\exp(-\eta F/RT)$ as shown in Figure 21, gives the following straight line equation.

$$\frac{1}{i} = 1.45 \times 10^{-6} \exp\left(\frac{-F\eta}{RT}\right) + 1.94 \quad (47)$$

The values of θ_0/i_r and i_0 are obtained by comparing the above expression with the equation 36. Substituting these values, into the equation 34, and considering $\theta = 1$, the limiting current density is deduced as follows.

$$1.94 i_L = 1$$

$$i_L = 0.52 \text{ A/cm}^2$$

The above value of the limiting current density, 0.52 A/cm^2 is within the range of experimentally observed limiting current density range of 0.50 to 0.71 A/cm^2 . The limiting current phenomenon can be explained in a similar way to that of previous case (Li_2CO_3), as it is mainly due to the absorption and desorption behavior of CO_x products.

5.0. COMPARISON OF $\text{LiF-CaF}_2 + \text{Li}_2\text{O}$ AND $\text{LiF-CaF}_2 + \text{Li}_2\text{CO}_3$ SYSTEMS

5.1. Solubility

The solubility of both Li_2O and Li_2CO_3 in LiF-CaF_2 melt exhibit similar behavior. It increases with temperature for both. However, in general the solubility level of Li_2O is higher than Li_2CO_3 for the same temperature levels. At 1093 K, the solubility level of Li_2O is 13.20 wt %, whereas the solubility Li_2CO_3 is 7.57 wt % in the same system. In many of the electrolytic production of reactive metals, it can be noted that even a solubility level of 2 wt % to 4 wt % of the respective oxides were found to be sufficient for the extraction of the elements. Even in the case of well established Hall-Herault process of aluminum electrowinning, the amount Al_2O_3 dissolved in the cryolite melt is about 5-10 wt %, during the normal operation of the cell. Therefore, the solubility levels exhibited by Li_2CO_3 , even though lower than Li_2O , should be sufficient enough for the electrolysis to extract lithium into the alloy phase. In the case of Li_2O , the electrolysis might be more efficient since its solubility is much higher.

5.2. Liquidus Temperatures

The liquidus temperature is another parameter that need to be considered in selecting a system for the electrochemical processes. The liquidus temperature of $\text{LiF-CaF}_2 + \text{Li}_2\text{O}$ (saturated) was reported to be 1006 K whereas for the $\text{LiF-CaF}_2 + \text{Li}_2\text{CO}_3$ (saturated) system it was found to be 1037 K. Therefore, the operational temperature of electrolyte with Li_2O , is lower compared to the electrolyte with Li_2CO_3 . This factor indicates again, a higher efficiency for the process utilizing the electrolyte with Li_2O .

5.3. Anodic Overvoltages

The comparison of the overvoltage measurements made at 1093 K indicates, that Li_2O saturated electrolyte exhibited lower overvoltages and Li_2CO_3 saturated electrolyte exhibited higher overvoltages for the same current density levels. The energy consumed per unit mass of the metal dissociated will be relatively higher in the case of electrolyte containing Li_2CO_3 . In general, higher the current density, greater will be the current efficiency of any electrolytic process. Therefore, the current density must be maintained to a very high value. However, it can not be raised to unlimited levels. It is determined by the limiting current density. Above this value, the anode effect comes into picture and results in difficulties for the operation of the cell as explained earlier in section 4.3.2. In the case of Li_2CO_3 saturated electrolyte, the limiting current density is very low when compared to the electrolyte saturated with Li_2O . Hence, electrolysis of Li_2O in the electrolyte might be again more efficient due to this high current density levels that can be achieved.

6. SUMMARY AND CONCLUSIONS

1. The solubility of Li_2O in LiF-CaF_2 electrolyte was determined by the Electromotive force method (EMF). It was found to increase from 11.42 wt % at 1078 K to 14.77 wt % at 1133 K.
2. Solubility measurements made by EMF method are in good agreement with the chemical analysis method. The activity coefficients were calculated based on solubility data, using conventional and Temkin's approaches. It was found that solubility Li_2O exhibited a negative deviation from ideality and Temkin's approach showed less deviation from ideal behavior.
3. The liquidus temperature of electrolyte saturated with Li_2CO_3 was determined to be 1037 K. The solubility of Li_2CO_3 increased from 2.95 wt % at 1063 K to 7.57 wt % at 1093 K.
4. The activities of Li_2CO_3 in LiF-CaF_2 were calculated from the solubility data using Temkin approach for ionic melts. Activities exhibited a negative deviation from Temkin's ideality. The solubility of Li_2CO_3 is lower than Li_2O in electrolyte at all the comparable temperature levels.
5. The anodic overvoltage vs Log current density measured on the graphite electrode showed a linear relationship at all temperatures studied.
6. The linear regression equation obtained for the overvoltage of $\text{LiF-CaF}_2 + \text{Li}_2\text{O}$ (sat) melt is $\eta = 1.32 + 0.84 \log i$. The limiting current density deduced for this system is 0.52 A/cm^2 .

7. The overvoltages on the graphite anode in $\text{LiF-CaF}_2+\text{Li}_2\text{CO}_3$ (saturated) melts showed a linear relationship as $\eta = 4.17 + 1.38 \log i$. The limiting current density value is 0.011 A/cm^2 .
8. In both systems, a charge transfer reaction between the oxyfluoride complex and the graphite electrode was proposed and the existence of the complexes LiOF^{2-} and $\text{Li}_2\text{OF}^{2-}$ were predicted. The stirring effect was found to have less effect and the limiting current phenomenon was mainly due to adsorption behavior of CO_x products on the electrode surface.
9. The current density values obtained for the system with Li_2O is much higher than the value of the system with Li_2CO_3 . Therefore, a higher current efficiency is predicted for the electrolysis of $\text{LiF-CaF}_2+\text{Li}_2\text{O}$ melts than $\text{LiF-CaF}_2+\text{Li}_2\text{CO}_3$.

7. SCOPE FOR FUTURE WORK

The liquidus temperature at which electrolysis is carried out is one of the important parameters that determines the efficiency of the process. One way of bringing down the liquidus temperature is adding other low melting fluoride salts in the electrolytes. Mixture of fluoride and chloride salts can be used to take advantage of the properties of both systems. Therefore, both these approaches are recommended to reduce the operation temperature.

The solubility of other low melting lithium compounds such as LiOH may be studied and compared with the other systems. The natural lithium silicate minerals can be used as a lithium source directly which eliminates the processing costs of intermediate lithium compounds. It has been predicted that electrolysis of $\text{LiF-CaF}_2+\text{Li}_2\text{CO}_3$ system would be less efficient from the liquidus temperatures and current density values. However, actual electrolysis experiments need to be conducted to confirm this.

It is also suggested that, the anodic overvoltage measurements and electrolysis experiments need to be carried out on the electrolyte containing different lithium sources including lithium silicate minerals. Effect of the concentration of lithium compounds on the anodic overvoltages is another factor that need to be studied which may change the kinetics of the reaction mechanisms taking place at the electrodes. From these studies, the best suitable system can be selected and process parameters must be optimized.

The second stage of the future work involves, the evaluation of microstructure and mechanical properties of the alloy produced by this new method. The final goal is the alloy produced with better mechanical properties than another process methods.

The economic and cost analysis can be carried out to demonstrate the commercial viability of the process. Aluminum and lithium are not the only elements present in the alloy. There are always other elements added for various property improvements. Therefore, processing of the multicomponent alloy system must also be investigated using this new process. If above mentioned tasks are fulfilled, then the possibility of processing other alloy systems such as Mg-Li, Al-Zn, Cu-Be etc., can also be investigated in the future by this new process.

1. W. K. Miller, A. J. Gorman, A. P. Trethewey and D. A. Thomas, Proc. International Symposium on Magnesium Alloys II, T. H. Sanders and E. A. Starke, Jr., eds., TMS-AIME, Warrendale, PA, 1983, pp. 25-32.
2. C. J. Pao, B. Dwyer, E. A. Starke, D. A. Thomas, T. J. Simpson and H. M. Johnson, Proc. International Symposium on Magnesium Alloys II, T. H. Sanders and E. A. Starke, Jr., eds., TMS-AIME, Warrendale, PA, 1983, pp. 281-282.
3. M. Tani, M. Tani, S. J. Lee, M. H. Lee, D. G. Lee, L. K. Kimura and H. K. Kimura, Proc. International Symposium on Magnesium Alloys II, T. H. Sanders and E. A. Starke, Jr., eds., TMS-AIME, Warrendale, PA, 1983, pp. 413-416.
4. W. Wang and S. J. Lee, Proc. International Symposium on Magnesium Alloys II, T. H. Sanders and E. A. Starke, Jr., eds., TMS-AIME, Warrendale, PA, 1983, pp. 407-412.
5. G. H. Ray, S. J. Lee, S. F. Dier and W. E. Dietz, Proc. International Symposium on Magnesium Alloys II, T. H. Sanders and E. A. Starke, Jr., eds., TMS-AIME, Warrendale, PA, 1983, pp. 317-320.
6. ALUMINUM SPECIAL COATING - Aluminum & Magnesium Coating Company, Inc., MA, 1980-82, pp. 20, 25, 67.
7. E. A. Starke, Jr. and T. H. Sanders, ASM, Vol. 2, 1981, p. 74.
8. Proc. International Symposium on Magnesium Alloys II, T. H. Sanders and E. A. Starke, Jr., eds., TMS-AIME, Warrendale, PA, 1983, p. 15.
9. E. A. Starke, Jr. and S. J. Lee, Proc. International Symposium on Magnesium Alloys II, T. H. Sanders and E. A. Starke, Jr., eds., TMS-AIME, Warrendale, PA, 1983, pp. 54-55.

REFERENCES

1. The New Materials Society: U.S. Department of Interior, Bureau of Mines, Vol.2, 1990, p.5.68.
2. M.W.Hunt., ed., Adv. Mater. & Processes: Vol.47, No.1, January 1995, p.7.
3. R.J.Rioja and R.H.Graham: Adv. Mater. & Processes, Vol.41, No.6, 1992, pp.23-26.
4. I.G.Palmer, R.E.Lewis, D.D.Crooks, E.A.Starke, Jr., and R.E.Crooks: Proc. aluminum-lithium Alloys II, T.H.Sanders and E.A.Starke, Jr., eds., TMS-AIME, Warrendale, PA, 1983, pp.91-110.
5. W.S.Miller, A.J.Cornish, A.P.Titchener and D.A.Bennett : Proc. aluminum-lithium Alloys II, T.H.Sanders and E.A.Starke, Jr., eds., TMS-AIME, Warrendale, PA, 1983, pp.335-362.
6. C.J.Peel, B.Evans, C.A.Baker, D.A.Bennett, P.J.Gregson and H.M.Flower : Proc. aluminum-lithium Alloys II, T.H.Sanders and E.A.Starke, Jr., eds., TMS-AIME, Warrendale, PA, 1983, pp.363-392.
7. B.van den Brandt, P.J.van den Brink, H.F.de Jong, L.Katgerman and H.Kleinjan: Proc. aluminum-lithium Alloys II, T.H.Sanders and E.A.Starke, Jr., eds., TMS-AIME, Warrendale, PA, 1983, pp.433-446.
8. W.Wang and N.J.Grant : Proc. aluminum-lithium Alloys II, T.H.Sanders and E.A.Starke, Jr., eds., TMS-AIME, Warrendale, PA, 1983, pp.447-468.
9. G.H.Narayanan, B.L.Wilson and W.E.Quist : Proc. aluminum-lithium Alloys II, T.H.Sanders and E.A.Starke, Jr., eds., TMS-AIME, Warrendale, PA, 1983, pp.517-542.
10. Alfa-AESAR, Product Catalog: Johnson & Matthey Catalog Company, Inc., MA, 1994-96, pp.292-299, 674.
11. E.A.Starke, Jr., and T.H.Sanders: JOM, Vol.8, 1981, p.24.
12. Yuki Kurihara: JOM, Vol.46, No.5, 1994, p.12.
13. E.S.Balmuth and R.Schmidt : Proc. aluminum-lithium Alloys, T.H.Sanders, Jr., and E.A.Starke, Jr., eds., TMS-AIME, Warrendale, PA, 1981, pp.69-88.

14. F.King: Aluminum and its alloys, Ellis Horwood Limited, Chichester, England, 1987, pp.146-147.
15. E.W.Lee, C.E.Nen and J.Kozol: JOM, Vol.42, No.5, 1990, pp.11-14.
16. A.P.Divecha and S.D.Karmarkar: Adv. Mater. & Processes, Vol.130, 1986, pp.75-79.
17. D.Webster: Adv. Mater.& Processes, Vol.145, No.5, 1994, pp.18-24.
18. G.LeRoy and Ph.Meyer: Proc. aluminum-lithium Alloys, R.J.Kar, S.P.Agrawal and W.E.Quist, eds., ASM International, Metals Park, OH, 1988, pp.77-154.
19. J.Thonstad, F.Nordmo and J.B.Paulsen: Metall. Trans. Vol.3, 1972, pp.403-408.
20. G.Winkhaus: TMS Paper Selection, Paper No: A 70-25, The Metallurgical Society of AIME, NY, 1970, pp.1-11.
21. W.E.Haupin: Proc.Light Metals-1979, W.S.Peterson, eds., TMS-AIME, NY, 1979, pp.353-361.
22. G.Picard, F.Seon, B.Tremillon and Y.Bertaud: Electrochim.Acta., Vol.25, 1980, pp.1453-1462.
23. M.P.Borom, R.H.Arendt and N.C.Cook: Ceramic Bulletin, Vol.60, No.11, 1981, pp.1168-1174.
24. C.M.Wai and M.Blander: Z.Naturforsch., Vol.39A, 1984, pp.499-502.
25. R.G.Reddy and S.G.Kumar: Metall. Mat. Trans.B, Vol.25B, 1994, pp.91-96.
26. H.Suito and D.R.Gaskell: Metall. Trans.B., Vol.7B, 1976, pp.559-566.
27. S.Shiying, Z.Keqi, Z.Yijing, Z.Minshon, B.Xiaojun, Z.Long and T.Dingsiang: Proc. Int. Conf. Rare Earth Development and Applications, X.Guangxian and X.Jimei, eds., Science Press, Beijing, PRC, September 1986, pp.1180-1184.
28. R.N.Seefuth and R.A.Sharma: J. Electrochem. Soc., Vol.135, No.4, 1988, pp.796-800.
29. T.Ishikawa, T.Sasaki, S.Konda, and M.Noguchi: Proc. Ninth Int. Symp. on Molten Salts, C.L.Hussey, D.S.Newman, G.Mamantov and Y.Ito, eds., The Electrochemical Society, Inc., Pennington, NJ, 1994, pp.164-170.

30. P.J.Tumidajski, M.Blander and D.S.Newman: *J. Electrochem. Soc.*, Vol.141, No.4, 1994, pp.895-900.
31. E.Morrice, E.S.Shedd and T.A.Henrie: USBM Rep. of Investigations, RI-7146, U.S. Dept. of the Interior, Bureau of Mines, Washington D.C., 1968, pp.1-12.
32. B.Porter and E.A.Brown: USBM Rep. of Investigations, RI-5878, U.S. Dept. of the Interior, Bureau of Mines, Washington D.C., 1961, pp.1-7.
33. H.Xiao, J.Thonstad and S.Rolseth: *Electrochemical Technology of Molten Salts*, Proc. of First European Workshop on Electrochemical Technology of Molten Salts, C.A.C.Sequeira and G.S.Picard, eds., Trans Tech Publ., Switzerland, 1993, pp.215-229.
34. C.Wai, I.Bloom, D.Caveny and M.Blander: *J.Phys.Chem.*, Vol.94, No.4, 1990, pp.1666-1669.
35. P.J.Tumidajski and M.Blander: *Molten Salt Chemistry and Technology: Proc. of Third Int. Symp. on Molten Salt Chemistry and Technology*, M.Chemla and D.Devilliers, eds., Trans Tech Publ., Switzerland, 1991, pp.250-272.
36. E.Morrice, B.Porter, E.A.Brown, C.Wyche and R.G.Knickerbocker: USBM Rep. of Investigations, RI-5868, U.S. Dept. of the Interior, Bureau of Mines, Washington D.C., 1961, pp.1-37.
37. E.Aamland, D.J.MacDonald and D.G.Kesterke: USBM Rep. of Investigations, RI-6226, U.S. Dept. of the Interior, Bureau of Mines, Washington D.C., 1963, pp.1-8.
38. D.G.Kesterke, D.C.Fleck and T.A.Henrie: USBM Rep. of Investigations, RI-6436, U.S. Dept. of the Interior, Bureau of Mines, Washington D.C., 1964, pp.1-12.
39. E.Morrice, C.Wyche and T.A.Henrie: USBM Rep. of Investigations, RI-6075, U.S. Dept. of the Interior, Bureau of Mines, Washington D.C., 1962, pp.1-9.
40. E.S.Shedd, J.D.Marchant and T.A.Henrie: USBM Rep. of Investigations, RI-6362, U.S. Dept. of the Interior, Bureau of Mines, Washington D.C., 1964, pp.1-11.
41. E.Morrice and T.A.Henrie: USBM Rep. of Investigations, RI-6957, U.S. Dept. of the Interior, Bureau of Mines, Washington D.C., 1967, pp.1-11.

42. D.K.Dysinger and J.E.Murphy: USBM Rep. of Investigations, RI-9504, U.S. Dept. of the Interior, Bureau of Mines, Washington D.C., 1994, pp.1-8.
43. J.Smolinski: J. Appl. Chem., Vol.6, 1956, pp.180-186.
44. J.Smolinski, J.C.Hannam and A.L.Leach: J. Appl. Chem., Vol.6, 1956, pp.187-196.
45. D.E.Kirby, D.A. O'Keefe and T.A.Sullivan: USBM Rep. of Investigations, RI-7629, U.S. Dept. of the Interior, Bureau of Mines, Washington D.C., 1972, pp.1-14.
46. M.F.Chambers and J.E.Murphy: Proc. of Symp. on Rare Earths, Extraction, Preparation and Applications, R.G.Bautista and M.M.Wong, eds., TMS Warrendale, PA, 1989, pp.369-376.
47. S.W.Chen, C.H.Jan, J.C.Lin and Y.A.Chang: Metall. Trans.A, Vol.20A, 1989, pp.2247-2258.
48. A.J.McAlister: Binary Alloy Phase Diagrams, Vol.1, T.B.Massalski, H.Okamoto, P.R.Subramanian, L.Kacprzak, eds., ASM International, Materials Park, OH, 1990, pp. 1,167,168.
49. W.E.Rocke: J. Electrochem. Soc., Vol.104, 1957, p.661.
50. S.G.Kumar, A.Narayan and R.G.Reddy: Proc. of Eighth Int. Symp. on Molten Salts, R.J.Gale, G.Blomgren and H.Kojima, eds., The Electrochemical Society, Inc., Pennington, NJ, 1992, pp.611-621.
51. R.G.Reddy and S.G.Kumar: Metall. Trans.B, Vol.24B, 1993, pp.1031-1035.
52. Y.K.Rao: Stoichiometry and Thermodynamics of Metallurgical Processes, Cambridge University Press, New York, NY, 1985, p.344.
53. P.T.Velu and R.G.Reddy: Proc. of EPD Congress 1994, TMS, Warrendale, PA, 1994, pp.1163-1169.
54. D.A.Jones: Principles and Prevention of Corrosion, Macmillan Publishing Company, New York, NY, 1992, pp.79-85.
55. D.R.Crow: Principles and Applicaitons of Electrochemistry, Chapman and Hall, London, U.K., 1988, pp.166-181.

56. A.R.Narayan: M.S. thesis., University of Nevada, Reno, NV, January 1988, pp.1-65.

APPENDIX - A

57. R.G.Reddy, A.R.Narayan and P.T.Velu: Proc. Ninth Int. Symp. on Molten Salts, C.L.Hussey, D.S.Newman, G.Mamantov and Y.Ito, eds., The Electrochemical Society, Inc., Pennington, NJ, 1994, pp.385-391.

(1) Calcium Fluoride

Suppliers: Fisher Chemical Co., J. Aldrich (St. Louis) Co.,

Composition	Wt % (max.)
Chloride	0.21
Arsenate	0.01
Sulfate	0.125
Barium	0.01
Heavy metals (as Pb)	0.0005
Loss	0.0015

(2) Lithium Fluoride

Suppliers: Fisher Chemical Co., Pure Metal Co.,

Composition	Wt % (max.)
Chloride	0.01
Arsenic (as As)	0.01
Sulfate	0.01
Barium	0.01
Heavy metals (as Pb)	0.0005

APPENDIX - A

Chemical Composition of the Salts Used

(1) Calcium Fluoride

Suppliers:- Fisher Chemical Co.,/ Aldrich Chemical Co.,

Composition	Wt % (max.)
Chloride	0.01
Ammonia	0.01
Sulfate	0.05
Barium	0.01
Heavy metals (as Pb)	0.005
Iron	0.005

(2) Lithium Fluoride

Suppliers:- Fisher Chemical Co.,/ Foote Mineral Co.,

Composition	Wt % (max.)
Chloride	0.01
Acidity (as HF)	0.02
Sulfate	0.01
Barium	0.01
Heavy metals (as Pb)	0.005

(10) Lithium Carbonate

(3) Lithium Oxide

Supplier:- Cerac Inc.,

Composition	Wt % (max.)
Assay	> 99.8
Aluminum	0.05
Barium	0.01
Calcium	0.02
Chromium	0.01
Copper	0.001
Iron	0.01
Magnesium	0.01
Silicon	0.01
Titanium	0.001
Strontium	0.001

(10) Silver Nitrate

Supplier:- Merck Chemical Co.,

Element	Composition
Copper	40 ppm
Iron	5 ppm
Magnesium	0.5 ppm
Silver	Remainder

(4) Lithium Carbonate

Supplier:- Fisher Chemical Co.,

Composition	Wt % (max.)
Assay	> 99.0
Chloride	0.005
Ammonium	5 ppm
Sulfar compounds	0.2
Nitrate	5 ppm
Heavy metals (as Pb)	0.002
Iron	0.002
Calcium	0.01
Potassium	0.01
Sodium	0.1

(5) Silver Fluoride

Supplier:- Aldrich Chemical Co.,

Assay 99.9 wt %

(6) Silver wire

Supplier:- Aldrich Chemical Co.,

Element	Composition
Copper	40 ppm
Iron	5 ppm
Magnesium	0.1 ppm
Silver	Remainder

APPENDIX - B**List of Publications**

1. P.T.Velu and R.G.Reddy: Proc. of EPD Congress 1994, ed. G.W.Warren, TMS, Warrendale, PA, 1994, pp.1163-1169.
2. R.G.Reddy, A.R.Narayan and P.T.Velu: Proc. Ninth Int. Symp. on Molten Salts, eds., C.L.Hussey, D.S.Newman, G.Mamantov and Y.Ito, The Electrochemical Society, Inc., Pennington, NJ, 1994, pp.385-391.
3. P.T.Velu and R.G.Reddy: Proc. of International Symposium on Extraction and Processing of Trace and Reactive Metals, eds., R.G.Reddy and B.Mishra, TMS, Warrendale, PA, 1995, pp.71-80

